Biomaterials 34 (2013) 2773–2786

Contents lists available at SciVerse ScienceDirect

Biomaterials

journal homepage: www.elsevier.com/locate/biomaterials

Intracellular delivery and antitumor effects of pH-sensitive liposomes based on zwitterionic oligopeptide lipids

Ran Mo, Qiong Sun, Nan Li, Can Zhang*

Center of Drug Discovery, State Key Laboratory of Natural Medicines, China Pharmaceutical University, Nanjing 210009, PR China

ARTICLE INFO

Article history:
Received 20 November 2012
Accepted 4 January 2013
Available online 23 January 2013

Keywords:
pH-sensitivity
Zwitterionic oligopeptide lipid
Liposomes
Drug delivery
Antitumor efficacy

ABSTRACT

pH-sensitive liposomes ($HHG2C_{18}$-L and $PEGHG2C_{18}$-L) based on zwitterionic oligopeptide lipids as anticancer drug carriers were developed and evaluated for effective intracellular delivery and enhanced antitumor activity. The amino acid-based lipids, 1,5-dioctadecyl-L-glutamyl 2-histidyl-hexahydrobenzoic acid ($HHG2C_{18}$) and 1,5-distearyl *N*-(*N*-α-(4-mPEG2000) butanedione)-histidyl-L-glutamate ($PEGHG2C_{18}$), were synthesized, which have the multistage pH-response to tumor microenvironmental pH (pH_e, pH 6.0–7.0) and endosomal/lysosomal pH (pH_i, pH 4.0–6.0) successively. $HHG2C_{18}$-L contains $HHG2C_{18}$, while $PEGHG2C_{18}$-L includes $HHG2C_{18}$ and $PEGHG2C_{18}$. Both of them displayed the capability of charge conversion to the surrounding pH. The zeta potentials of $HHG2C_{18}$-L and $PEGHG2C_{18}$-L were negative at pH 7.4, whereas positive at pH 6.5 and more positive at lower pH. Coumarin 6-loaded $HHG2C_{18}$-L (C6/$HHG2C_{18}$-L) and $PEGHG2C_{18}$-L (C6/$PEGHG2C_{18}$-L) showed higher tumor cellular uptake due to electrostatic absorptive endocytosis at pH_e (pH 6.5), produced proton sponge effect for endo-lysosomal escape, and accumulated to the mitochondria based on stronger positive charge by the hydrolysis of a pH-sensitive linker at pH_i (pH 5.5 and pH 4.5). Furthermore, temsirolimus (CCI-779)-loaded $HHG2C_{18}$-L (CCI-779/$HHG2C_{18}$-L) and $PEGHG2C_{18}$-L (CCI-779/$PEGHG2C_{18}$-L) had significantly higher antiproliferative and apoptosis inducing effects toward the human renal carcinoma (A498) cells at pH 6.5 relative to that at pH 7.4. The half maximal inhibitory concentration (IC50) of CCI-779/$HHG2C_{18}$-L and CCI-779/$PEGHG2C_{18}$-L were about 3 μg/mL and 5 μg/mL at pH 6.5, 1.67-fold and 1.60-fold improved relative to that at pH 7.4, respectively. The total apoptotic ratio of CCI-779/$HHG2C_{18}$-L and CCI-779/$PEGHG2C_{18}$-L increased from 9.90% and 7.78% at pH 7.4 to 19.53% and 12.10% at pH 6.5, respectively. *In vivo*, CCI-779/$PEGHG2C_{18}$-L after intravenous administration presented remarkably higher bioavailability and blood persistence compared with unPEGylated CCI-779/$HHG2C_{18}$-L, and had the strongest antitumor efficacy against xenograft renal cancer (Renca) tumor models. Accordingly, the results provide the feasibility of using pH-sensitive zwitterionic oligopeptide lipids to extend the applications of liposomes to efficient anticancer drug delivery in cancer therapy.

1. Introduction

Liposomes, lipid vesicles, have been demonstrated as substantially promising carriers for a large range of applications in tumor-targeted drug and gene delivery [1–3], and additionally have been clinically and preclinically employed for cancer therapy, such as Doxil® [4] and DaunoXome® [5]. They present improved plasma stability of anticancer drugs and considerable retention in the blood, thereby contributing to an efficient delivery of their cargos to the target tissues. Liposomes with a diameter smaller than 200 nm accumulate at the tumor tissues by the enhanced permeability and retention (EPR) effect based on the salient characteristics of the tumor vascular architecture [6]. A myriad of the stable liposomes are internalized by the tumor cells, followed by an endocytic pathway to finally transfer into the endosomes/lysosomes for degradation, resulting in an inferior antitumor efficacy [7]. Accordingly, a liposomal delivery system is still highly desirable to attain an optimal pharmaceutical effect, in which the endocytic liposomes can flee from the endosomes/lysosomes before degradation.

Cationic liposomes have the capability of facilitating the tumor cellular uptake by the electrostatic absorptive endocytosis [8,9], since the cell membranes possess an overall negative charge resulted from the presence of sialic acid and proteoglycan. More significantly, after internalization, cationic liposomes tend to fuse

* Corresponding author. Tel./fax: +86 25 83271171.
E-mail address: zhangcancpu1801@yahoo.com.cn (C. Zhang).

0142-9612/$ – see front matter © 2013 Elsevier Ltd. All rights reserved.
http://dx.doi.org/10.1016/j.biomaterials.2013.01.030

with the endosomal/lysosomal membrane under the assistance of specific lipids for membrane fusion to release their contents into the cytoplasm [10–12], or perform the proton sponge effect similar to polyethylenimine (PEI) leading to the swelling and disruption of the endosomes/lysosomes for cytoplasmic liberation of the intact liposomes [13,14]. Of note, the latter mode is able to be used for potentially further subcellular targeting, including nuclear or mitochondrial targeting. Despite these advantages, for intravenous administration, positively charged nanoparticles including cationic liposomes cause severe cytotoxicity, serum inhibition and a rapid clearance from the reticuloendothelium system (RES) as a result of aggregation with plasma proteins [15].

In view of this, introduction of a poly(ethylene glycol) (PEG)-modified lipid (PEG-lipid) into the cationic liposomal membrane is a common approach for application of cationic liposomes *in vivo*, which cannot completely eliminate but partially diminish the net surface charge and the interaction with opsonin for increased half-life in the blood. Nevertheless, PEGylation impaired the interaction between the liposomes and the tumor cells, thereby reducing the tumor cellular uptake, after the arrival of the liposomes at the tumor site [16]. Accordingly, more studies have paid attention to the liposomes functionalized with a PEG deshielding mechanism by a degradable pH-sensitive bond between PEG and lipid, such as hydrazone bonds [17–19]. Actually, almost all of these pH-sensitive bonds degrade at pH much lower than the tumor extracellular pH (pH_e, pH 6.0–7.0), suggesting that PEG may not shed from the liposomal surface at the tumor microenvironment but generally in the intracellular endosomal/lysosomal pH (pH_i, pH 4.0–6.0), which indicates no or little ability to improve the cellular uptake at the tumor milieu. Moreover, the degradation of the pH-sensitive bonds is a kind of chemical reaction, which is typically a gradual not instantaneous process. Obata et al. developed the pH-responsive liposomes containing synthetic glutamic acid-based zwitterionic lipids, which can quickly change surface charge from negative to positive at pH_i, producing efficient release of drugs in the cytoplasm by membrane fusion [20]. However, these liposomes still presented negative charge at pH_e and had no effect on subcellular targeting.

In order to integrate the merits of anionic liposome for lower hematotoxicity, PEGylated liposomes for longer circulation in the blood, and cationic liposomes for enhanced uptake at the tumor site and efficient intracellular delivery in the tumor cells, we developed pH-sensitive zwitterionic oligopeptide liposomes ($HHG2C_{18}$-L and $PEGHG2C_{18}$-L) based on two synthetic amino acid-based lipids, 1,5-dioctadecyl-L-glutamyl 2-histidyl-hexahydrobenzoic acid ($HHG2C_{18}$) and 1,5-distearyl *N*-(*N*-α-(4-mPEG2000) butanedione)-histidyl-L-glutamate ($PEGHG2C_{18}$), which endue the liposomes with multistage pH-response to tumor extracellular matrix and intracellular compartment. $HHG2C_{18}$-L contains $HHG2C_{18}$, while $PEGHG2C_{18}$-L includes $HHG2C_{18}$ and $PEGHG2C_{18}$ (Fig. 1). The pH-sensitive liposomes present negative charge in the blood, and reverse charge to positive triggered by pH_e at the tumor site to increase tumor cellular uptake by electrostatic absorptive endocytosis. In the endosomes/lysosomes, the imidazole group of histidine in $HHG2C_{18}$ and $PEGHG2C_{18}$ develops the proton sponge effect for endosomal/lysosomal escape, and hexahydrobenzoic amide hydrolyses induced by pH_i to provide the liposomes with a stronger positive surface charge by the loss of carboxyl groups in $HHG2C_{18}$ for mitochondrial targeting to induce cell apoptosis, due to the high mitochondrial membrane potential (MMP) up to approximately 130–150 mV (negative inside).

We have previously demonstrated the high performance of $HHG2C_{18}$-L for mitochondrial-targeted drug delivery [21]. The present investigation is to further confirm that $HHG2C_{18}$-L encapsulating drugs have the effect on initiating the mitochondrial apoptotic pathway, and more importantly, to evaluate that $PEGHG2C_{18}$-L not only remains the multistage pH-response of $HHG2C_{18}$-L for effective intracellular trafficking and antiproliferation *in vitro*, but also exhibits improved bioavailability and blood persistence *in vivo* for higher antitumor efficacy than $HHG2C_{18}$-L.

2. Materials and methods

2.1. Materials

N,*N*-dicyclohexylcarbodiimide (DCC), triethylamine (TEA), succinic anhydride (SA) and 4-dimethylaminopyridine (DMAP) were purchased from Sinopharm Chemical Reagent Co. Ltd. (Shanghai, China). 1-hydroxybenzotrizole (HOBt) and *N*-hydroxysuccinimide (NHS) were obtained from Aladdin Reagent Inc. (Shanghai, China). Soy phosphatidylcholine (SPC) was offered by Taiwei Pharmaceutical Co., Ltd. (Shanghai, China). Cholesterol (Chol) was provided by Huixing Biochemical Reagent Co, Ltd. (Shanghai, China). Temsirolimus (CCI-779) was purchased from Xingcheng Chempharm Co., Ltd. (Taizhou, China). Methoxy poly(ethylene glycol) ($mPEG_{2k}$), coumarin 6 (C6), sucrose, amiloride and nystatin were purchased from Sigma–Aldrich Co. (Shanghai, China). RPMI-1640 medium (1640, Gibco®) and trypsin (Gibco®) were purchased from Pufei Bio-Technology Co., Ltd. (Shanghai, China). Fetal bovine serum (FBS, Hyclone®), penicillin–streptomycin solution (Hyclone®), phosphate buffered saline (PBS, Hyclone®) and 3-(4,5-dimethylthiazol-2-yl)-2,5-diphenyltetrazolium bromide (MTT) were provided by Sunshine Biotechnology Co., Ltd. (Nanjing, China). LysoTracker Red, Hoechst 33258 and mitochondrial membrane potential assay kit with JC-1 (5,5′,6,6′-tetrachloro-1,1′,3,3′-tetrethyl benzimidalyl carbocyanine iodide) and Annexin V-FITC apoptosis detection kit were purchased from Beyotime Institute of Biotechnology (Nantong, China). MitoTracker Red (Invitrogen®) was offered by Qcbio Science and Technologies Co., Ltd. (Shanghai, China). All other chemicals and reagents were analytical grade.

2.2. Synthesis and characterization of PEGylated zwitterionic oligopeptide lipid

$HHG2C_{18}$ was synthesized as described in detail elsewhere (Fig. S1A) [21], and $PEGHG2C_{18}$ was synthesized as follows (Fig. S1B). $mPEG_{2k}$ (10.0 g, 5.0 mmol), SA (4.0 g, 40.0 mmol) and DMAP (0.6 g, 5.0 mmol) were dissolved in chloroform (200 mL), and refluxed for 12 h at 60 °C. After removing chloroform, the reactant was dissolved in 5% $NaHCO_3$, followed by washing by acetic ether (20 mL × 3) to remove unreacted SA. The pH of the $NaHCO_3$ solution was adjusted to pH 2–3 by 1 M HCl, and the solution was extracted by dichloromethane. After dry with anhydrous sodium sulfate, 4-mPEG-4-oxobutanoic acid (mPEGS) with a yield of 91.4% was obtained by removing dichloromethane. Subsequently, mPEGS (5.0 g, 2.4 mmol), DCC (1.5 g, 7.2 mmol) and NHS (0.6 g, 4.8 mmol) were dissolved in chloroform (50 mL) with stirring for 3 h, followed by adding the synthesized 1,5-dioctadecyl *N*-(*N*-g-tosyl) histidyl-L-glutamate ($H(Tos)G2C_{18}$) (2.3 g, 2.4 mmol) and TEA (0.3 g, 2.6 mmol) chloroform solution (50 mL) with further stirring for 12 h. The reaction mixture was washed with distilled water (15 mL × 3), dried with anhydrous sodium sulfate, and isolated by column chromatography to gain the amino group-protected intermediate ($PEGH(Tos)G2C_{18}$) with a yield of 44.1%. $PEGH(Tos)G2C_{18}$ (3.2 g, 1.1 mmol) and HOBt (1.8 g, 13.2 mmol) were dissolved in tetrahydrofuran (40 mL) with stirring for 5 h at room temperature. $PEGHG2C_{18}$, a white powder with a yield of 41.1%, was obtained from the resulting solution above by chromatography separation, followed by the rotary evaporation.

2.3. Preparation and characterization of liposomes

Zwitterionic oligopeptide liposomes, $HHG2C_{18}$-L and $PEGHG2C_{18}$-L, were prepared by a film dispersion method followed by membrane extrusion. $HHG2C_{18}$-L was fabricated by SPC, $HHG2C_{18}$ and Chol (7.5:2.5:1, w:w:w), while conventional liposomes (SPC-L) were prepared with SPC and Chol (10:1, w:w). 2.5% (w:w) CCI-779 and 0.076% (w:w) C6 of the total lipids were added to the liposomal composition to construct the drug-loaded and fluorescence-labeled liposomes, respectively. $PEGHG2C_{18}$ (1 mol% or 5 mol%) was added in the lipid components of $HHG2C_{18}$-L to produce $PEGHG2C_{18}$-L. Lipids were dissolved in the mixture of chloroform and methanol (2:1, v:v). After the organic solvents were removed by the rotary evaporation at 40 °C, a thin lipid film formed and was further dried under vacuum overnight to remove any traces of remaining solvents. Subsequently, the lipid film was hydrated in 5 mL of Milli-Q® water (Milli-Q Reagent Water System, Millipore, USA) at 37 °C. Liposomes were dispersed by using an ultrasonic cell disruptor (LifeScientz Bio-tech Co. Ltd., China), and then extruded repeatedly through polycarbonate membrane filters with a pore size of 0.22 μm.

The encapsulation efficiency (EE) was calculated by the following formula: $EE = W/W_0 \times 100\%$, where W and W_0 are the amounts of drugs in the liposomes after and before passing over Sephadex G-50 column, respectively.

The drug-loading capacity (DL) was calculated by the following formula: $DL = W_{drug}/W_{lipid} \times 100\%$, where W_{drug} and W_{lipid} are the amounts of drugs and lipids in the resulting liposomes, respectively.

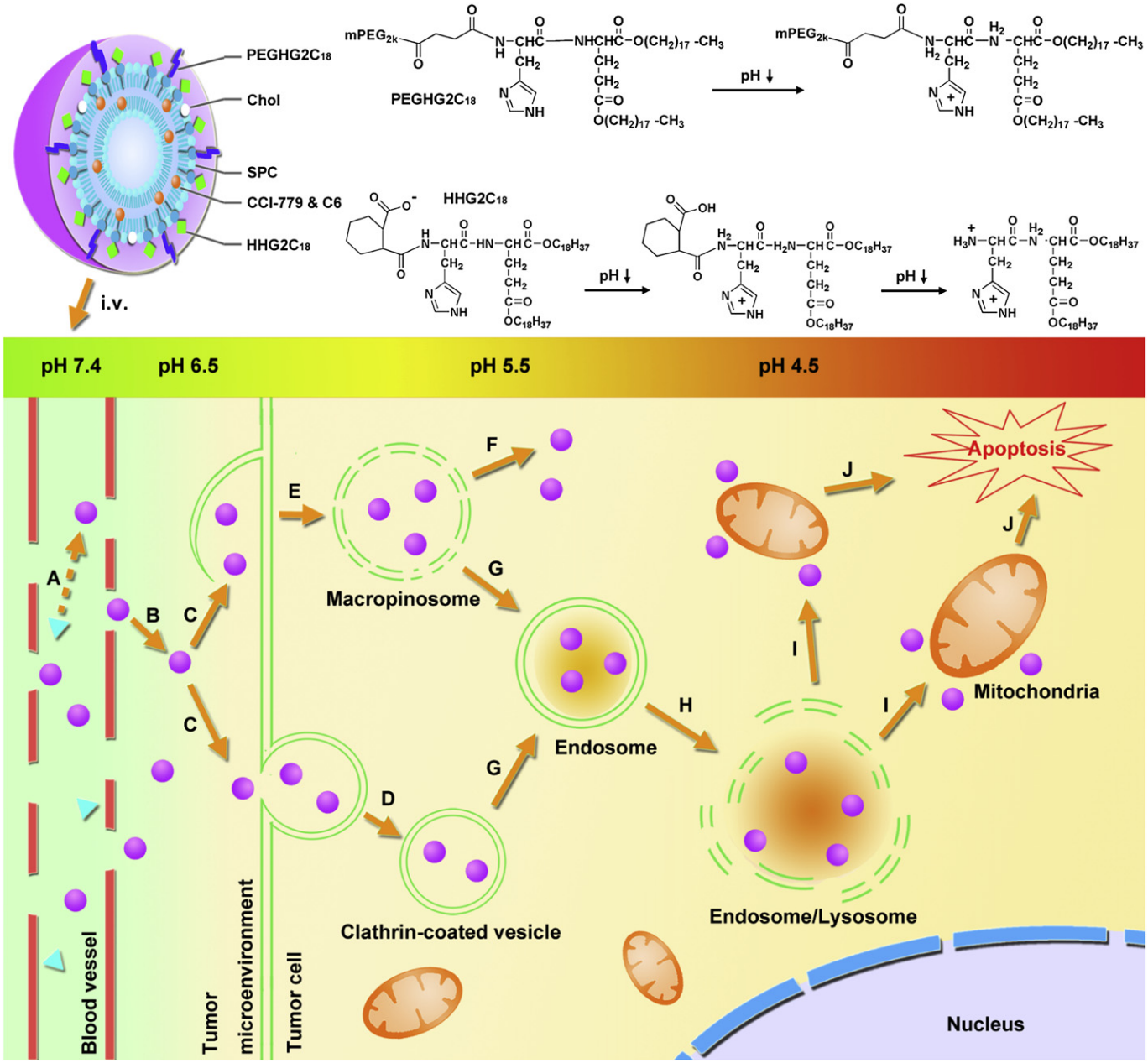

Fig. 1. Schematic design of representative PEGylated zwitterionic oligopeptide liposomes (PEGHG2C$_{18}$-L), which compose of soy phosphatidycholine (SPC), cholesterol (Chol) and two synthesized amino acid-based zwitterionic lipids (PEGHG2C$_{18}$ and HHG2C$_{18}$). PEGHG2C$_{18}$ and HHG2C$_{18}$ can respond to tumor extracellular and intracellular pH to endue PEGHG2C$_{18}$-L with efficient intracellular delivery and enhanced antitumor efficacy. (A) The PEG outer corona and negatively charged surface provide a good protection for liposomes (purple sphere) away from the attack of plasma proteins (blue triangle) in the blood. (B) Targeting of liposomes through EPR effect. (C) Charge conversion from negative to positive for enhanced cellular uptake at tumor pH. (D) Clathrin-mediated endocytosis. (E) Macropinocytosis. (F) Leakage of liposomes from the porous macropinosomes. (G) Delivery to endosomes. (H) Endosomal/Lysosomal escape as a result of the proton sponge effect. (I) Cytoplasmic liberation and subsequent mitochondrial targeting. (J) Promotion of cell death via mitochondrial apoptotic pathway. (For interpretation of the references to colour in this figure legend, the reader is referred to the web version of this article.)

200 μL of the liposomes was diluted in 3 mL of Milli-Q® water, and the mean particle diameter and polydispersity index (PDI) were then measured by a Dynamic Light Scattering Analyzer (Brookhaven, USA).

2.4. pH-sensitive charge conversion and hexahydrobenzoic amide hydrolysis

To demonstrate pH-sensitive charge conversion of HHG2C$_{18}$-L and PEGHG2C$_{18}$-L to the surrounding pH, we measured the zeta potential of HHG2C$_{18}$-L and PEGHG2C$_{18}$-L dispersed in the buffer solutions at different pH values (pH 7.4, 6.5, 5.5, 4.5), respectively. 150 μL of the liposomes was diluted in 3 mL of 20 mM Hepes buffer (pH 7.4) or 20 mM acetate buffer (pH 4.5, 5.5, 6.5) to the total lipid concentration of 1.2 mg/mL. The zeta potentials and particle sizes of the resulting liposomes at various pH values were measured at 37 °C by a ZetaPlus Zeta Potential Analyzer (Brookhaven, USA).

To explore the acid-labile hydrolysis of hexahydrobenzoic amide, the zeta potential of HHG2C18-L and PEGHG2C$_{18}$-L was assayed after incubation with the buffer solutions at different pH values (pH 7.4, 6.5, 5.5, 4.5) for different time, respectively. 1 mL of the liposomes was incubated with 2 mL of 20 mM Hepes buffer (pH 7.4) or 20 mM acetate buffer (pH 6.5, 5.5, 4.5) at 37 °C. At predetermined time intervals (0, 2, 4, 6, 8, 12, 24 h), 300 μL of each sample was added into 2 mL of the buffer solution to the total lipid concentration of 1.2 mg/mL at the same pH value. The zeta potentials of the resulting liposomes at various pH values were measured at 37 °C by a ZetaPlus Zeta Potential Analyzer.

2.5. Cell culture

Human renal carcinoma (A498) cells and murine renal carcinoma (Renca) cells were cultured in 1640 with 10% (v:v) FBS, 100 U/mL penicillin and 100 μg/mL

streptomycin in an incubator (Thermo Scientific, USA) at 37 °C under an atmosphere of 5% CO_2 and 90% relative humidity. The cells were subcultivated approximately every 3 days at 80% confluence using 0.25% (w:v) trypsin at a split ratio of 1:5.

2.6. Cellular uptake and endocytosis pathways

A498 cells (1×10^5 cells/well) were seeded and used for the uptake assays in 24-well plates after 48 h. To investigate the effect of charge conversion of HHG2C_{18}-L and PEGHG2C_{18}-L on enhancing tumor cellular uptake, different C6-loaded liposomes (C6/SPC-L, C6/HHG2C_{18}-L, C6/PEGHG2C_{18}-L) were diluted in the FBS-free culture medium with different pH values (pH 7.4 and pH 6.5) to C6 concentration of 100 ng/mL. After cell incubation with different C6-loaded liposomes at 37 °C for 2 h, the cells were washed by 4 °C PBS thrice, and the amount of C6 was assayed by HPLC. The cellular uptake of C6 was calculated as the following equation. Uptake of C6 (ng/mg) = $Q_{C6}/Q_{\text{cell proteins}}$, where Q_{C6} and $Q_{\text{cell proteins}}$ were the amounts of C6 and cell proteins, respectively.

To estimate the endocytosis pathways of the liposomes, the cells were first cultured with different specific agents for various kinds of endocytosis (inhibitor of clathrin-mediated endocytosis: sucrose (154 mg/mL) [22]; inhibitor of caveolin-mediated endocytosis: nystatin (15 μg/mL) [23]; inhibitor of macropinocytosis: amiloride (133 μg/mL) [24]) for 1 h at 37 °C. Subsequently, uptake study was performed in the presence of the agent and C6-loaded liposomes at C6 concentration of 100 ng/mL for 2 h at 37 °C. The cells were washed by 4 °C PBS thrice. The amount of C6 was assayed by HPLC, and the uptake of C6 was calculated.

2.7. Intracellular delivery

The intracellular delivery of the liposomes in A498 cells, such as endosomal/lysosomal escape and mitochondrial targeting, was evaluated by confocal laser scanning microscopy (CLSM) (Olympus, Japan) and flow cytometry (Becton Dickinson, USA), respectively.

The double-labeling experiment was carried out by using CLSM to observe the cytoplasmic distribution of the liposomes in A498 cells. The localization of different C6-loaded liposomes (C6/SPC-L, C6/HHG2C_{18}-L, C6/PEGHG2C_{18}-L) was visualized by labeling the cells with different specific fluorescent probes such as LysoTracker and MitoTracker. The cells (1×10^5 cells/well) were seeded in a special confocal microscopy dish (Greiner Bio-One, Germany) for 24 h at 37 °C, followed by cell incubation with different C6-loaded liposomes at C6 concentration of 100 ng/mL. At prearranged time intervals (1, 4, 8, 12 h), the cells were washed by 4 °C PBS thrice, and then stained with organelle-selective dye. Lysosomes and mitochondria were stained with 50 nM LysoTracker Red and 200 nM MitoTracker Red for 30 min at 37 °C, respectively. Subsequently, the cells were washed by PBS thrice and observed by CLSM.

To quantitatively assess mitochondrial targeting of the liposomes, C6 content in the mitochondrial fraction was quantified by flow cytometry. The cells (1×10^5 cells/well) were seeded in 6-well plates for 48 h at 37 °C, and incubated with different C6-loaded liposomes (C6/SPC-L, C6/HHG2C_{18}-L, C6/PEGHG2C_{18}-L) at C6 concentration of 1 μg/mL for 12 h. Subsequently, the cells were washed by 4 °C PBS twice and then trypsinized. Trypsinization was stopped by adding 4 °C complete culture medium. After centrifugation at 600× g for 5 min, the cells were washed twice by 4 °C PBS. The isolation of mitochondria was performed according to the guide of mitochondria isolation kit (Beyotime, China). Briefly, the cells were resuspended in the mitochondria isolation buffer (provided in the kit) and subjected to 20 strokes in a Dounce homogenizer to give a homogenate. The homogenate solution was centrifuged at 600× g for 10 min. The supernatant was then centrifuged at 11,000× g for 10 min to pellet the mitochondria. The pelleted mitochondrial fraction was resuspended in 4 °C PBS, and analyzed by flow cytometry.

2.8. Antiproliferation in vitro

In vitro antiproliferation of different CCI-779-loaded liposomes (CCI-779/SPC-L, CCI-779/HHG2C_{18}-L, CCI-779/PEGHG2C_{18}-L) against A498 cells at pH 7.4 and pH 6.5 was estimated by using MTT assay. The cells (1×10^4 cells/well) were seeded in 96-well plates. After culture for 24 h, the cells were exposed to the FBS-free culture medium adjusted to pH 7.4 or pH 6.5 containing different CCI-779-loaded liposomes with various CCI-779 concentrations for 48 h, followed by adding 20 μL of MTT solution (5 mg/mL). After 4 h, the medium was removed, and the cells were mixed with 150 μL of dimethyl sulfoxide (DMSO). The absorbance was measured at 570 nm by a microplate reader (Thermo Scientific, USA).

2.9. Cell apoptosis

The effect of different CCI-779-loaded liposomes (CCI-779/SPC-L, CCI-779/HHG2C_{18}-L, CCI-779/PEGHG2C_{18}-L) on cell apoptosis was evaluated by observing morphous of stained cell nuclei, measuring MMP and using Annexin V-FITC apoptosis detection, respectively.

Hoechst staining of nuclei was used to observe morphological changes of cancer cells. A498 cells (1×10^5 cells/well) were seeded in 6-well plates for 48 h at 37 °C, and incubated with different CCI-779-loaded liposomes at CCI-779 concentration of 20 μg/mL for 12 h. The cells were washed by 4 °C PBS twice, fixed by paraformaldehyde (4% w/v) for 10 min and then stained by Hoechst 33258 for 5 min. After washing by 4 °C PBS twice, the cells were observed by fluorescence microscope (Olympus, Japan).

Variation in MMP was analyzed using MMP assay kit with JC-1 by flow cytometry. A498 cells (1×10^5 cells/well) were seeded in 6-well plates for 48 h at 37 °C, and incubated with different CCI-779-loaded liposomes at CCI-779 concentration of 20 μg/mL for 12 h. The cells were washed by 4 °C PBS twice, followed by trypsinizing. Trypsinization was stopped by adding 4 °C complete culture medium. After centrifugation at 600× g for 5 min, the cells were washed by 4 °C PBS twice, incubated with JC-1 staining solution for 20 min at 37 °C, and washed by 4 °C blank staining solution twice. Subsequently, the cells were resuspended with the blank staining solution, and analyzed by flow cytometry.

Apoptotic cell death was determined by using Annexin V-FITC apoptosis detection kit, according to the manufacturer's protocol. Briefly, A498 cells (1×10^5 cells/well) were seeded in 6-well plates for 48 h at 37 °C, and then incubated with the CCI-779-loaded liposomes at CCI-779 concentration of 20 μg/mL at pH 6.5 and pH 7.4 for 12 h, respectively. The cells were harvested, washed by 37 °C PBS twice, and suspended in the binding buffer. 5 μL of Annexin V-FITC was added into the cell suspensions for 15 min incubation, and then 5 μL of propidium iodide (PI) was added. The cells were immediately analyzed by flow cytometry.

2.10. Animals and tumor xenograft models

Male Sprague-Dawley (SD) rats (180–220 g) and male Kunming (KM) mice (20–25 g) were purchased from College of Veterinary Medicine Yangzhou University (Jiangsu, China). All the animals were pathogen free and allowed to access food and water freely. The experiments were carried out in compliance with the National Institute of Health Guide for the Care and Use of Laboratory Animals.

To set up the tumor xenograft model, mice were subcutaneously inoculated in the back with Renca cells (1×10^7 cells) suspended in PBS (20 μL). Tumor volume (V) was determined by measuring length (L) and width (W), and calculated as $V = L \times W^2/2$. Tumor-bearing mice were used as the volumes of tumor reached around 100 mm^3 at Day 8 post-tumor inoculation.

2.11. Pharmacokinetics studies

SD rats were weighed and randomly divided into four groups ($n = 4$), and received intravenous injection of Torisel®, CCI-779/SPC-L, CCI-779/HHG2C_{18}-L and CCI-779/PEGHG2C_{18}-L at a dose of 10 mg/kg. After administration, blood samples were collected at 0.083, 0.167, 0.25, 0.5, 1, 2, 4, 6, 8, 12, 24 h, and then centrifuged at 10,000× g for 10 min. The supernatant plasma was obtained and stored at −20 °C until HPLC analysis.

The pharmacokinetic parameter of each CCI-779 formulation was calculated using a non-compartmental model by Kinetica 4.4 (Thermo, USA), such as the area under the plasma concentration-time curve ($AUC_{0-\infty}$), elimination half-life ($t_{1/2}$) and mean residence time (MRT).

2.12. Antitumor efficacy in vivo

Renca tumor-bearing mice were weighed and randomly divided into five groups ($n = 10$) as the volumes of tumor reached around 100 mm^3 at Day 8 post-tumor inoculation, and received Torisel®, CCI-779/SPC-L, CCI-779/HHG2C_{18}-L and CCI-779/PEGHG2C_{18}-L at a dose of 10 mg/kg and saline as control. Different formulations of CCI-779 were administrated intravenously at Day 8, 9, 10, 11, 12, 15 and 16. Tumor size and body weight of the tumor-bearing mice were measured every day. At Day 22 post-tumor inoculation, mice were sacrificed and the tumors were separated and sectioned for histological evaluation with hematoxylin and eosin (HE) staining. The survival rates were monitored throughout the study.

2.13. CCI-779 and C6 quantification by HPLC

The HPLC system comprised of an LC-20AB pump, SPD-M20A diore array detector, RF-10AXL fluorescence detector, SIL-20AC autosampler and CTO-20A column oven (SHIMADZU, Japan). An Inertsil® ODS-SP column (250 mm × 4.6 mm × 5 μm, GL Sciences Inc., Japan) was employed for the separation of analytes at a flow rate of 1 mL/min. For CCI-779, the column temperature was 50 °C and the wavelength was set at 276 nm. The mobile phase was consisted of methanol and water at 83:17 (v:v) for entrapment efficiency assay and at 76:24 (v:v) for pharmacokinetics and biodistribution determination. For C6, the column temperature was 35 °C. The excitation and emission wavelength were set at 467 nm and 503 nm, respectively. The mobile phase composed of methanol and ammonium acetate buffer (20 mM, pH 4.0) (95:5, v:v).

C6 concentrations in the cells were analyzed by HPLC described above. Briefly, the cells in the cell plates were disrupted by 200 μL of cell lysis buffer (Beyotime, China) to release the drug in the cells. The cell suspension was obtained in lysis buffer by blowing air repeatedly and gently. After centrifugation at 10,000× g for 5 min, 20 μL of supernatant was used for BCA protein assay (Beyotime, China) to quantitate the cell proteins. In addition, 50 μL of supernatant was mixed with 200 μL

Table 1
Particle size, polydispersity index (PDI), entrapment efficiency (EE) and drug-loading capacity (DL) of various liposomes.

Liposomes	Particle size (nm)	PDI	EE (%)	DL (%)
Bare SPC-L	92.6 ± 0.70	0.206 ± 0.006	N/A	N/A
CCI-779/SPC-L	100.8 ± 6.74	0.224 ± 0.002	95.24 ± 3.58	2.16 ± 0.08
C6/SPC-L	94.4 ± 1.30	0.234 ± 0.004	98.35 ± 16.07	0.077 ± 0.012
Bare $HHG2C_{18}$-L	100.4 ± 0.70	0.212 ± 0.004	N/A	N/A
CCI-779/ $HHG2C_{18}$-L	134.5 ± 1.66	0.227 ± 0.006	96.70 ± 5.49	2.20 ± 0.12
C6/$HHG2C_{18}$-L	104.5 ± 1.30	0.229 ± 0.008	93.76 ± 7.39	0.071 ± 0.006
Bare $PEGHG2C_{18}$-L	123.7 ± 0.60	0.167 ± 0.003	N/A	N/A
CCI-779/ $PEGHG2C_{18}$-L	151.1 ± 13.70	0.172 ± 0.015	95.72 ± 9.83	1.83 ± 0.19
C6/$PEGHG2C_{18}$-L	125.0 ± 10.00	0.181 ± 0.012	91.42 ± 2.40	0.058 ± 0.002

of methanol, vortexed for 5 min, and centrifuged at 10,000× g for 10 min. 20 μL aliquots of the supernatant were injected into the HPLC system.

CCI-779 concentrations in the plasma were also analyzed by HPLC described above. 100 μL of plasma was mixed with 200 μL of acetonitrile, vortexed for 5 min, and centrifuged at 10,000× g for 10 min. 20 μL aliquots of the supernatant were injected into the HPLC system.

2.14. Statistical analysis

Data are given as mean ± standard deviation. Statistical significance was tested by two-tailed Student's *t*-test or one-way ANOVA. Statistical significance was set at $^{*}P < 0.05$, and extreme significance was set at $^{**}P < 0.01$.

3. Results and discussion

3.1. Preparation and characterization of liposomes

The conventional SPC-L as pH-insensitive liposomes consisted of SPC and Chol. $HHG2C_{18}$, with the similar structure to the natural phospholipids containing the hydrophilic head group and the hydrophobic tail group, was anchored into the membrane of SPC-L to construct $HHG2C_{18}$-L, and $PEGHG2C_{18}$-L was prepared by adding $PEGHG2C_{18}$ (1 mol% or 5 mol% of total lipids) into the formulation of $HHG2C_{18}$-L. Both of CCI-779, an anti-renal cancer drug and C6,

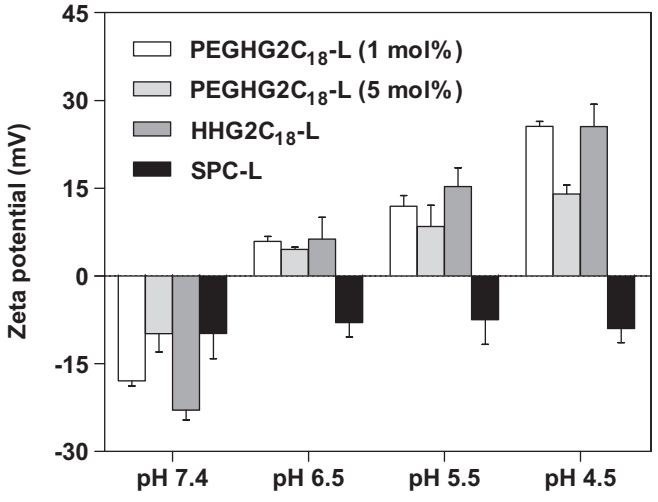

Fig. 2. Zeta potential of SPC-L, $HHG2C_{18}$-L and $PEGHG2C_{18}$-L at different pH values.

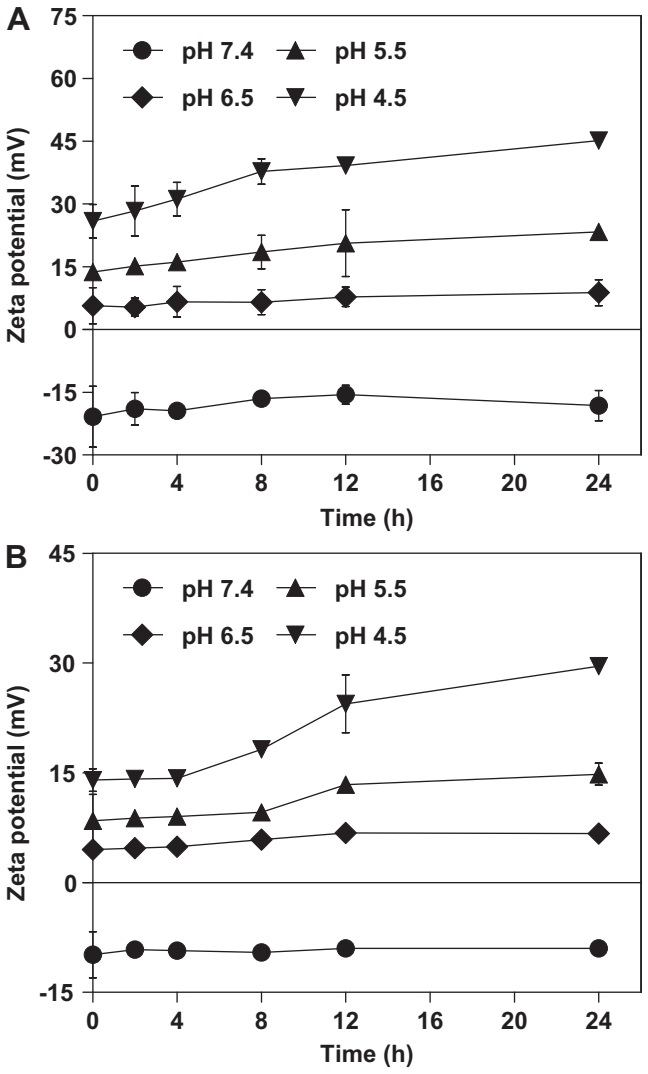

Fig. 3. Zeta potential variation of $HHG2C_{18}$-L (A) and $PEGHG2C_{18}$-L (B) accompanied by the hydrolysis of the hexahydribenzoic amide at different pH values for different time.

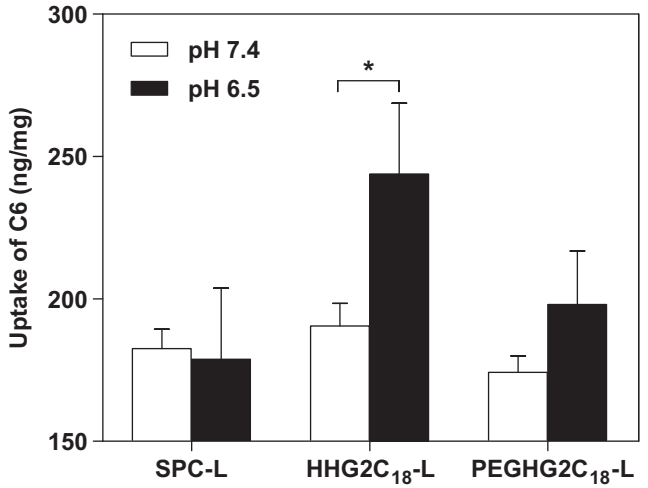

Fig. 4. Cellular uptake of C6/SPC-L, C6/$HHG2C_{18}$-L and C6/$PEGHG2C_{18}$-L on A498 cells at pH 7.4 and pH 6.5. Uptake of C6 is the ratio between the amount of C6 in the cells (ng) and the cell proteins (mg). $^{*}P < 0.05$.

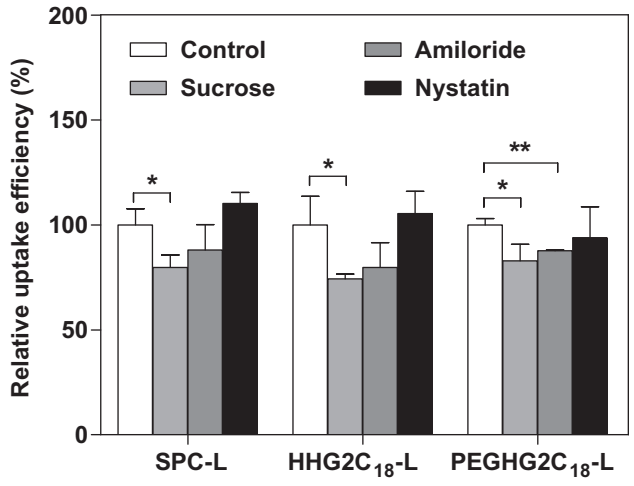

Fig. 5. Relative uptake efficiency of C6/SPC-L, C6/HHG2C_{18}-L and C6/PEGHG2C_{18}-L on A498 cells in the presence of various endocytosis inhibitors. Sucrose, amiloride, and nystatin are the inhibitors for the clathrin-mediated endocytosis, macropinocytosis and caveolin-mediated endocytosis, respectively. $^{*}P < 0.05$, $^{**}P < 0.01$.

a fluorescent tracer were hydrophobic and encapsulated into the liposomal phospholipid bilayers. Table 1 showed the particle size, PDI, EE, and DL of different liposomes. Both HHG2C_{18}-L and PEGHG2C_{18}-L had larger sizes, compared with the bare SPC-L with a particle size of 92.6 ± 0.70 nm. Herein, PEGHG2C_{18}-L showed a larger diameter (123.7 ± 0.60 nm) with a better polydispersity (0.167 ± 0.003) than HHG2C_{18}-L owing to the PEG hydration layer, which is consistent with many reported PEGylated nanoparticles (NPs) [25,26]. Hydrophobic CCI-779 and C6 were efficiently encapsulated in the lipid bilayer of the liposomes. EE and DL of CCI-779 in the liposomes were higher than 90% and 2%, respectively. Compared with the bare liposomes, CCI-779- and C6-loaded liposomes had larger particle sizes resulted from drug encapsulation in the lipid bilayer of the liposomes. The concentration of the total lipids, CCI-779 and C6 in the liposomes were about 24 mg/mL, 0.6 mg/mL and 0.02 mg/mL, respectively.

3.2. pH-sensitive charge conversion

To demonstrate that the zwitterionic oligopeptide lipids endue HHG2C_{18}-L and PEGHG2C_{18}-L with pH-sensitive charge conversion to the surrounding pH, the zeta potential of different liposomes at various pH values were measured. The pH values of 7.4, 6.5, 5.5 and

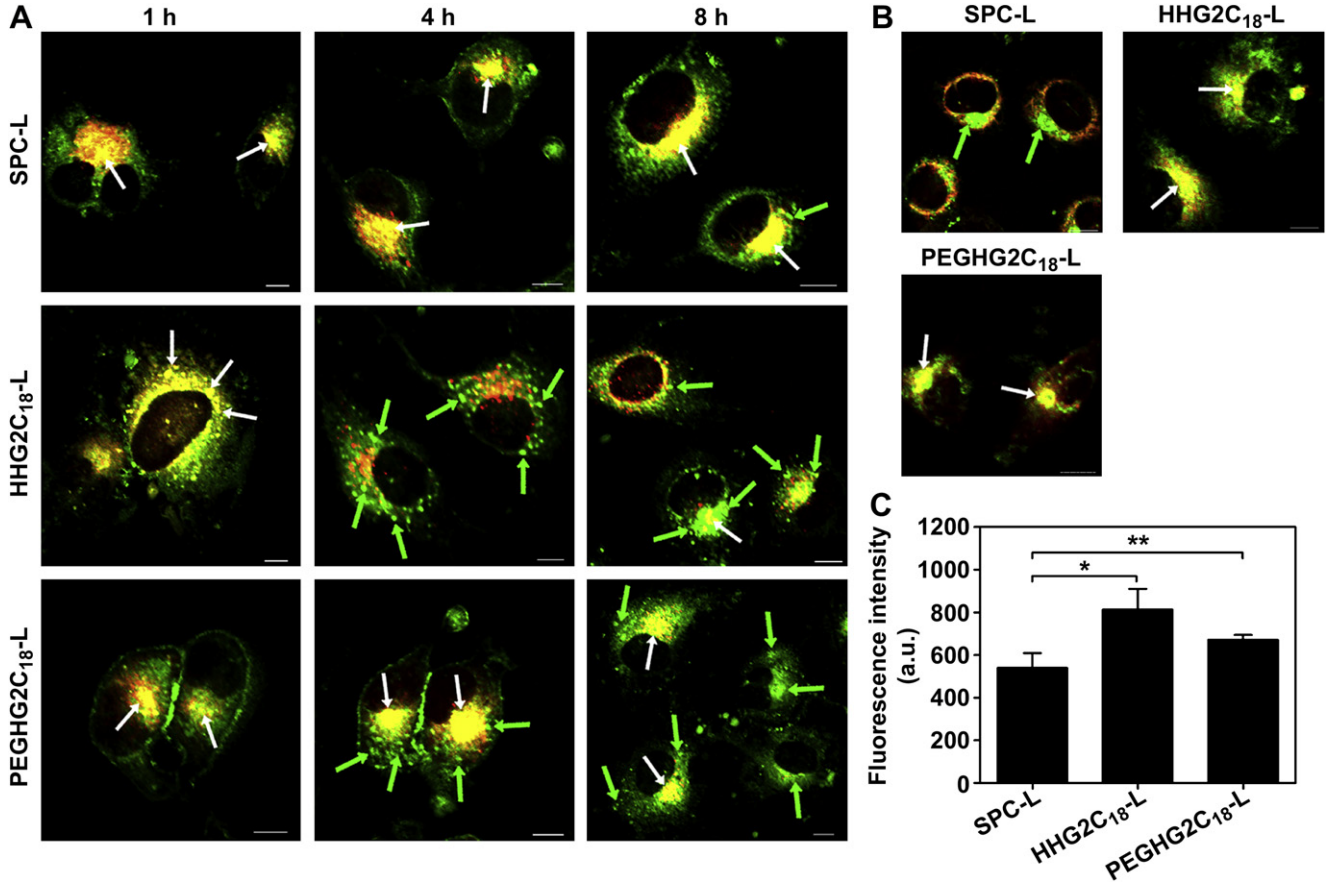

Fig. 6. (A) Intracellular delivery of C6/SPC-L, C6/HHG2C_{18}-L and C6/PEGHG2C_{18}-L on A498 cells at different time (1, 4, 8 h) observed by CLSM. The late endosomes and lysosomes were stained by LysoTracker Red. White arrows signify the occasions of coincidence between the liposomes and the endosomes/lysosomes. Green arrows indicate the liposomes escaping from the endosomes/lysosomes into the cytoplasm. Scale bars are 10 μm. The separate CLSM images of C6-loaded liposomes and the endosomes/lysosomes are shown in Fig. S2. (B) Colocalization of C6/SPC-L, C6/HHG2C_{18}-L and C6/PEGHG2C_{18}-L into the mitochondria of A498 cells at 12 h observed by CLSM. The mitochondria were stained by MitoTracker Red. White arrows represent the occasions of coincidence between the liposomes and the mitochondria. Green arrows signify the liposomes with no mitochondriotropics. Scale bars are 10 μm. The separate CLSM images of C6-loaded liposomes and the mitochondria are shown in Fig. S3. (C) Fluorescence intensities of the mitochondria isolated from A498 cells treated with C6/SPC-L, C6/HHG2C_{18}-L and C6/PEGHG2C_{18}-L for 12 h by flow cytometry. $^{*}P < 0.05$. (For interpretation of the references to colour in this figure legend, the reader is referred to the web version of this article.)

4.5 simulated that of physiological condition, tumor milieu, endosomal and lysosomal compartment, respectively. As shown in Fig. 2, the zeta potential of the pH-insensitive SPC-L remained constantly negative regardless of pH value. However, the zeta potential of $HHG2C_{18}$-L was more negative (-22.92 ± 1.68 mV) at pH 7.4 due to the introduction of more carboxyl groups of $HHG2C_{18}$ on the liposomal surface, and interestingly, it promptly changed to positive ($+6.32 \pm 3.73$ mV) at pH 6.5 over the narrow pH range of 7.4–6.5, which is mainly attributed to the protonation/deprotonation of amino and carboxyl groups. Furthermore, $HHG2C_{18}$-L presented a concomitant increase of the positive charge with the increasing acidity. The zeta potential of $HHG2C_{18}$-L continuously rose to $+15.30 \pm 3.19$ mV at pH 5.5 and $+25.53 \pm 3.79$ mV at pH 4.5.

Similarly, $PEGHG2C_{18}$-L presented the capability of charge conversion toward pH as well, although the hydration shell of PEG had a certain effect on shielding surface charge of $HHG2C_{18}$-L as reported [27,28]. Both 1 mol% and 5 mol% PEGylation almost decreased the zeta potential of $HHG2C_{18}$-L at all the pH values. The strength of charge shielding effect of PEG showed a positive correlation with the amount of $PEGHG2C_{18}$. The zeta potential of $PEGHG2C_{18}$-L with 5 mol% PEGylation was much lower than that with 1 mol% PEGylation and $HHG2C_{18}$-L. Differently, 1 mol% $PEGHG2C_{18}$-L showed the zeta potential at pH 4.5 ($+25.56 \pm 0.83$ mV) equivalent to $HHG2C_{18}$-L ($+25.53 \pm 3.79$ mV), which indicates no shielding effect of PEG at such a low pH value. The main reason is that $PEGHG2C_{18}$-L contains more imidazole rings of histidines introduced by $PEGHG2C_{18}$ compared with $HHG2C_{18}$-L, which are able to highly protonate at pH 4.5 for increased positive surface charge, and the PEG hydration layer of 1 mol% $PEGHG2C_{18}$ falls short of charge shielding, while that of 5 mol% is adequate to reduce the surface positive charge at pH 4.5 ($+14.00 \pm 1.56$ mV). No change in the particle sizes of $HHG2C_{18}$-L and $PEGHG2C_{18}$-L at different pH values was found (Table S1). Theoretically, for the PEGylated liposomes with the size of about 100 nm, PEG is arranged in the mushroom mode with <4 mol% PEGylation, in the transition configuration with 4–8 mol%, and in the brush conformation with >8 mol%. It is difficult to prepare the brush-mode PEGylated liposomes due to their disruption by detergent-like PEGylated amphiphiles [29]. Additionally, Doxil®, a clinical liposomal formulation, contains 5 mol% of PEG with the molecular weight of 2000. To ensure the stability and improve the pharmacokinetics of the PEGylated liposomes, pH-sensitive $PEGHG2C_{18}$-L with 5 mol% $PEGHG2C_{18}$ was employed for further investigations.

Based on these results, $HHG2C_{18}$-L and $PEGHG2C_{18}$-L had the ability to change the zeta potential according to the environmental pH, which is attributed to the chemical structure of the zwitterionic lipid including the carboxyl group of hexahydrobenzoic acid and the amino group of histidine. It is confirmed that charge conversion of $HHG2C_{18}$-L and $PEGHG2C_{18}$-L from negative to positive occurs at pH_e and endues them with stronger positive charge at pH_i.

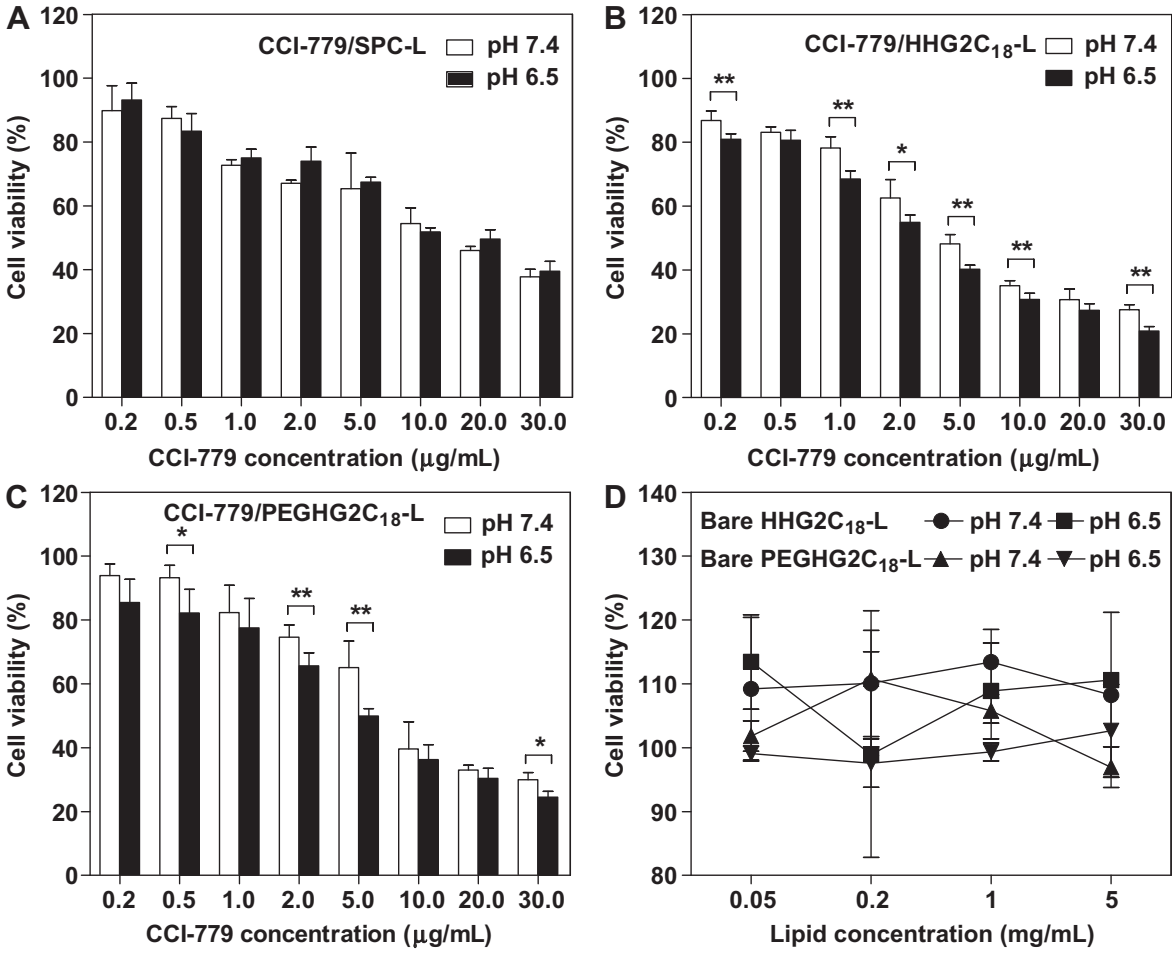

Fig. 7. A–C) Antiproliferative activity of CCI-779/SPC-L (A), CCI-779/$HHG2C_{18}$-L (B) and CCI-779/$PEGHG2C_{18}$-L (C) on A498 cells at pH 7.4 and pH 6.5 for 48 h. $^{*}P < 0.05$, $^{**}P < 0.01$. (D) Cytotoxicity of bare $HHG2C_{18}$-L and $PEGHG2C_{18}$-L with different lipid concentrations toward A 498 cells at pH 7.4 and pH 6.5 for 48 h.

3.3. pH-sensitive hydrolysis of hexahydrobenzoic amide

Apart from mitochondrial targeting signal peptides (MTS), mitochondrial targeting is generally dependent upon the electrostatic interaction between positively charged NPs and mitochondria, which have high MMP approximately up to 130–150 mV (negative inside). However, charge conversion of NPs is only based on protonation/deprotonation of the amino and carboxyl groups, which indicates that these NPs escaping from endosomes/lysosomes to cytoplasm have surface charge reconversion from positive to negative, leading to the loss of interactions with the mitochondria. Acid-labile beta-carboxylic acid amides present pH-dependent hydrolysis compared with unsubstituted amides due to nucleophilic catalysis by the carboxylic acid. Reaction proceeds via an addition intermediate from which the amine is expelled, producing a cyclic anhydride as the second product [30,31]. To confirm the pH-sensitive hydrolysis of hexahydrobenzoic amide accompanied by the removal of carboxyl groups from the liposomes resulting in the liposomal positive charge increase, we measured the zeta potential of HHG2C$_{18}$-L and PEGHG2C$_{18}$-L at various pH values at different time, respectively.

As shown in Fig. 3, the resulting amide in HHG2C$_{18}$ exhibited a great degradability at pH 5.5 and pH 4.5 compared with at pH 7.4. The positive charge of HHG2C$_{18}$-L and PEGHG2C$_{18}$-L had a corresponding increase with the hydrolysis of the amide. The zeta potential of HHG2C$_{18}$-L gradually reached to about $+23.32 \pm 2.00$ mV at pH 5.5 and $+45.15 \pm 2.00$ mV at pH 4.5 in 24 h. By comparison, HHG2C$_{18}$-L showed a zeta potential of -18.22 ± 3.61 mV at pH 7.4 even after 24 h in consequence of the presence of carboxyl groups. Similarly, PEGHG2C$_{18}$-L presented the zeta potential of $+14.82 \pm 1.47$ mV at pH 5.5 and $+29.57 \pm 0.94$ mV at pH 4.5 in 24 h, compared with that of -8.98 ± 0.77 mV at pH 7.4. It is certified that the hexahydrobenzoic amide is prone to degrade in the endosomal/lysosomal compartments at pH$_i$ rather than at pH$_e$ or at physiological pH, resulting in the removal of carboxyl groups, avoiding the charge reconversion of the liposomes in the cytoplasm and laying a good foundation for subsequent mitochondrial targeting.

3.4. pH-dependent cellular uptake

In attempt to demonstrate that pH$_e$-triggered charge conversion facilitates tumor cellular uptake, A498 cells were incubated with different C6-loaded liposomes at pH 7.4 and pH 6.5, respectively. The *in vitro* released amount of C6 from all the liposomes was lower than 1% for 24 h regardless of pH value (data not shown), which suggests that most of uptake of C6 is laid to the uptake of the liposomes rather than that of free C6. As shown in Fig. 4, the cellular uptake of C6/HHG2C$_{18}$-L or C6/PEGHG2C$_{18}$-L at pH 6.5 was higher than that at pH 7.4, suggesting a pH-dependent uptake process of the liposomes. In contrast, the uptake of C6/SPC-L showed no noticeable change. The enhanced uptake of pH-sensitive liposomes at pH$_e$ was attributable in part to the electrostatically adsorptive endocytosis [32]. C6/PEGHG2C$_{18}$-L exhibited a lower cellular uptake as a result of reduced affinity to the cells by the PEG shell in comparison with C6/HHG2C$_{18}$-L regardless of pH value.

Recently, many investigations about pH-induced PEG deshielding to increase the cellular uptake were described. E. Koren et al. constructed a liposomal preparation containing TAT-peptide moieties, sterically shielded with a degradable pH-sensitive hydrazone bond between PEG chains and PE (PEG–Hz–PE conjugate). The liposomes lose their PEG coating by the hydrolysis of a hydrazone pH-sensitive bond at pH 5, and penetrate inside cells via the effect of exposed TAT-peptide moieties [33]. Y. Nie et al. also used the hydrazone bond to design pyridylhydrazone-based PEGylation for pH-reversible lipopolyplex shielding at pH 5.4 to increase the transfection efficiency [34]. In spite of these great advances, the majority of PEG deshielding

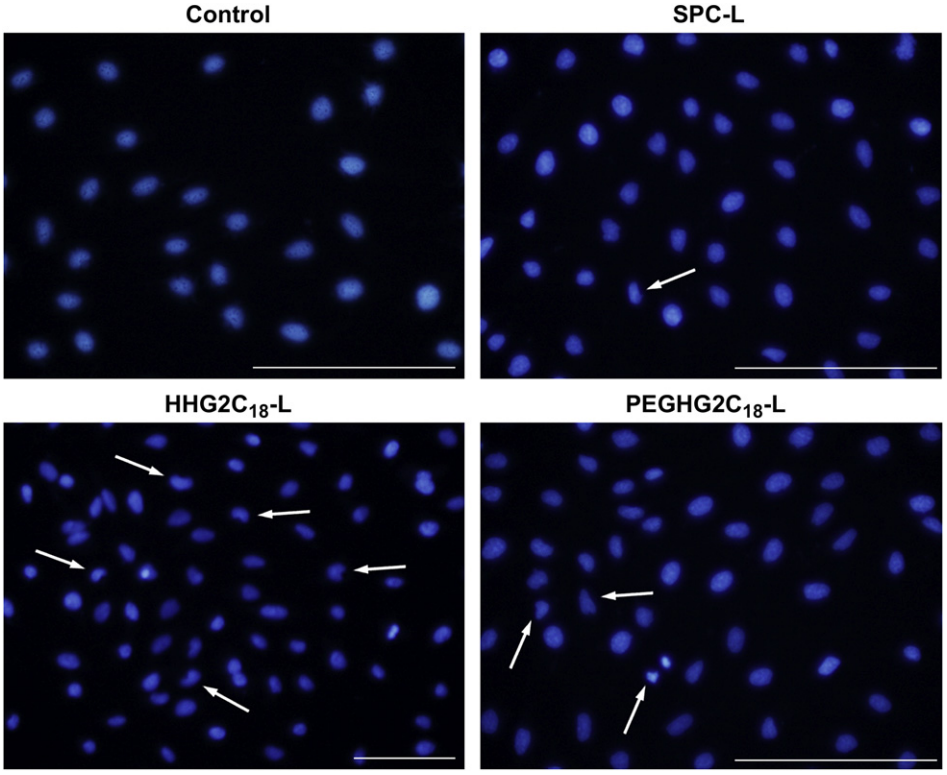

Fig. 8. Fluorescent images for nuclei shrinking and noticeable nuclear condensation (signified by white arrows) of A498 cells treated with CCI-779/SPC-L, CCI-779/HHG2C$_{18}$-L and CCI-779/PEGHG2C$_{18}$-L for 12 h. The nuclei were stained by Hoechst 33258. Scale bars are 50 μm.

for improved cellular uptake occurs at the pH value lower than pH_e as mentioned before. However, PEGHG2C$_{18}$-L without PEG deshielding is able to elevate the cellular uptake at pH 6.5 by means of charge conversion. More importantly, charge conversion of PEGHG2C$_{18}$-L is an instantaneous process for a prompt response to pH change, which differs from that PEG deshielding is relatively slower with a requisite reaction time in the degradation of the linker conjugating PEG.

3.5. Endocytosis pathways

Understanding the endocytosis pathways and the locations of the liposomes in the cells is important to clarify their intracellular trafficking for an appropriate targeting strategy. The internalization mechanism of different C6-loaded liposomes in A498 cells was evaluated by using various blockers of specific cellular internalization pathways, respectively. As shown in Fig. 5, all of the cellular uptake of different C6-loaded liposomes decreased remarkably in the presence of sucrose ($P < 0.05$), an inhibitor of clathrin-mediated endocytosis [22], whereas had no significant change in the presence of nystatin, an inhibitor of caveolin-mediated endocytosis [23], which indicates that they encounter the primary barrier, endosomes/lysosomes, in the intracellular delivery. Besides, the presence of amiloride, an inhibitor of macropinocytosis [24], also extremely reduced the cellular uptake of C6/PEGHG2C$_{18}$-L ($P < 0.01$), compared with C6/SPC-L and C6/HHG2C$_{18}$-L. It is speculated that PEGHG2C$_{18}$-L enters the cells initially in clathrin-coated vesicles and macropinosomes by clathrin-dependent endocytosis and macropinocytosis, respectively, and both further in endosomes/lysosomes. Of note, uptake through macropinocytosis is more efficient than that through clathrin-mediated endocytosis in terms of avoiding endosomal/lysosomal degradation resulting in an efficient drug delivery, since macropinosomes compared with clathrin-coated vesicles have a more porous membrane structure for enhanced leakage of inclusions into cytoplasm [35,36].

3.6. Intracellular delivery

The liposomes are actively internalized into tumor cells and encapsulated in endosomes/lysosomes, which are a primary obstruction for drug delivery owing to their bio-function of degrading substances internalized into the cells. Thus, we pay particular attention to whether HHG2C$_{18}$-L or PEGHG2C$_{18}$-L exhibits endosomal/lysosomal escape for cytoplasmic release. Double-labeling experiment for subcellular localization was performed by using CLSM. Lysosomes as well as late endosomes were selectively stained as a red fluorescence by LysoTracker Red, a specific marker for these acidic organelles, while the liposomes encapsulating C6 were observed as a green fluorescence. Colocalization of the liposomes with the specific organelle dyes was viewed as a yellow fluorescence. As shown in Fig. 6A, the overwhelming majority of the green fluorescence was highly overlaid with the red fluorescence when the cells were incubated with C6/SPC-L even for 8 h, demonstrating that it is difficult for the irresponsive SPC-L to penetrate through the endosomes/lysosomes. In contrast, the green fluorescence of C6/HHG2C$_{18}$-L and C6/PEGHG2C$_{18}$-L had an evident dissociation with the red fluorescence at 4 h, demonstrating their efficient endosomal/lysosomal escape, although both of them delivered into the endosomes/lysosomes by judging from the yellow fluorescence after A498 cell incubation for 1 h. At 8 h, they showed broader cytoplasmic release and distribution, followed by more effective endosomal/lysosomal escape, which is judging by the stronger green fluorescence and weaker red fluorescence. Furthermore, since the staining of the endosomes/lysosomes by the tracker was dependent on the acidity of the endosomal/lysosomal compartments, the red fluorescence of the endosomes/lysosomes got weaker (Fig. S2), which indicates the destruction of the acid endosomal/lysosomal environment as a result of the proton sponge effect of histidines in HHG2C$_{18}$-L and PEGHG2C$_{18}$-L in agreement with many previous reports [37–39].

Next, we are interested in further exploring translocation of the escaped HHG2C$_{18}$-L or PEGHG2C$_{18}$-L to the mitochondria and comparing their efficiency of mitochondrial targeting qualitatively and quantitatively. Double-labeling experiment was also carried out by using CLSM, in which the mitochondria were selectively stained as a red fluorescence by MitoTracker Red. Moreover, the C6 content in the isolated mitochondria was estimated by flow cytometry. As shown in Fig. 6B, the yellow fluorescence displayed that HHG2C$_{18}$-L and PEGHG2C$_{18}$-L escaped from the endosomes/lysosomes was specifically accumulated to the mitochondria in 12 h, while SPC-L had little mitochondriotropics by judging a large disassociation between the green and red fluorescence (Fig S3). On the other hand, as shown in Fig. 6C, the fluorescence intensity of C6 in the mitochondria isolated from A498 cells incubated with C6/HHG2C$_{18}$-L ($P < 0.05$) or C6/PEGHG2C$_{18}$-L ($P < 0.01$) was significantly higher than that incubated with C6/SPC-L for 12 h, which

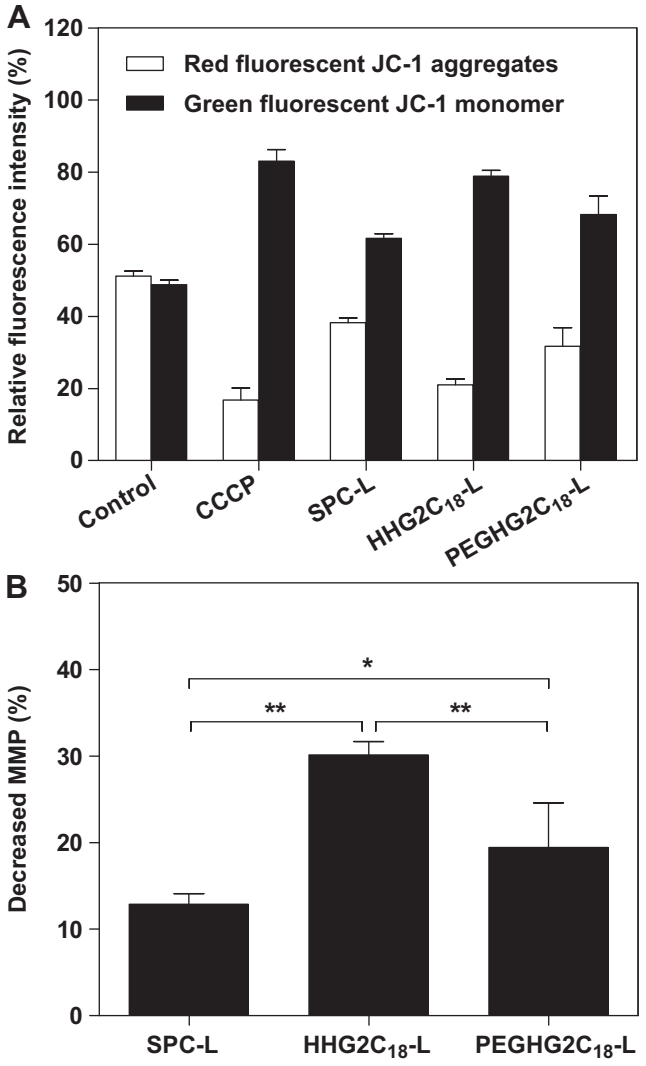

Fig. 9. Relative fluorescence intensity of JC-1 aggregates and monomer (A) and change in the mitochondrial membrane potential (MMP) (B) of A498 cells treated with CCI-779/SPC-L, CCI-779/HHG2C$_{18}$-L and CCI-779/PEGHG2C$_{18}$-L for 12 h by flow cytometry. $^{*}P < 0.05$, $^{**}P < 0.01$.

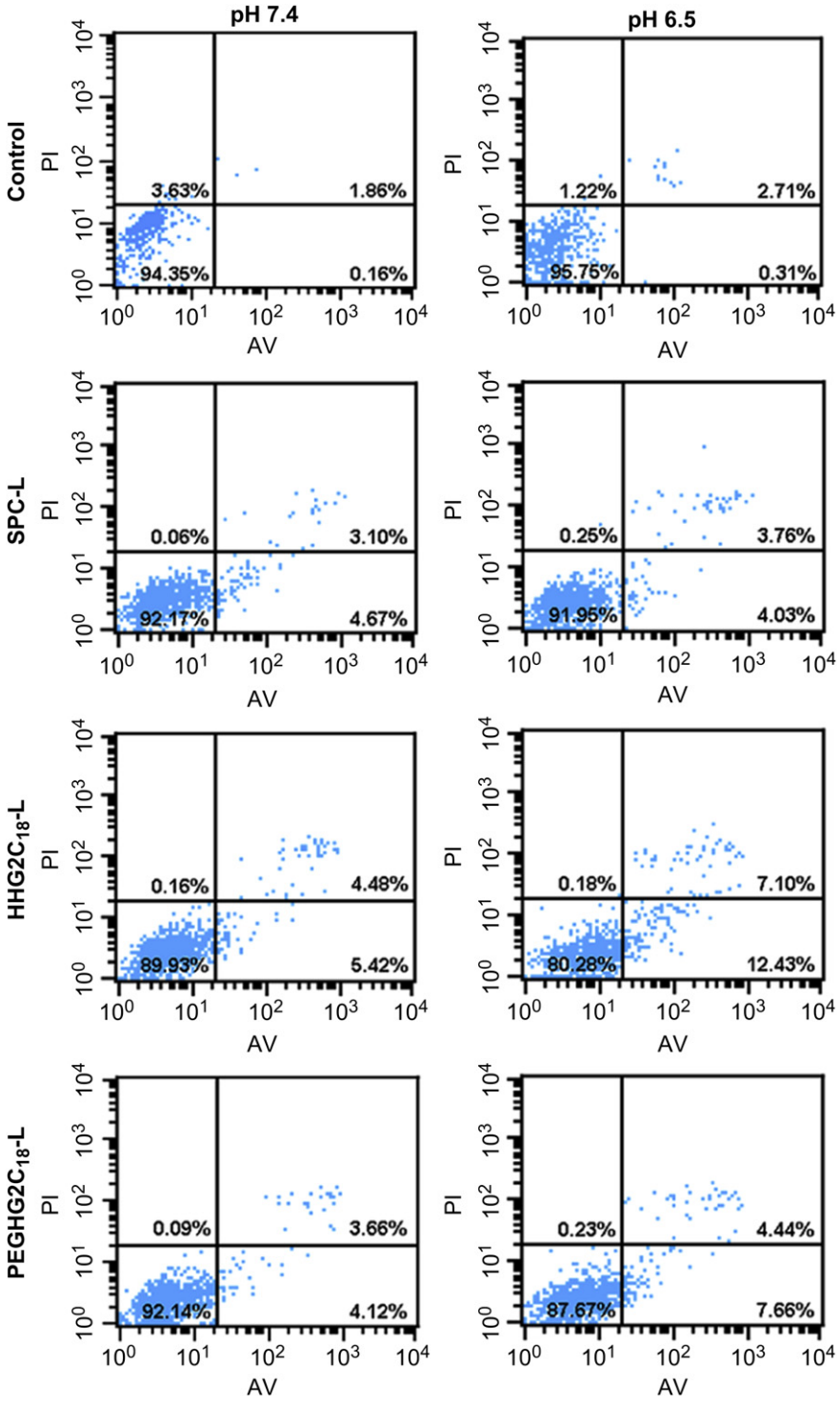

Fig. 10. Cell apoptosis induced by CCI-779/SPC-L, CCI-779/HHG2C_{18}-L and CCI-779/PEGHG2C_{18}-L at pH 7.4 and pH 6.5 for 12 h by using Annexin V-FITC/PI staining. In each panel, the lower-left (Annexin V-FITC$^-$, PI$^-$), lower-right (Annexin V-FITC$^+$, PI$^-$), and upper-right (Annexin V-FITC$^+$, PI$^-$) quadrants represent the populations of live cells, early apoptotic cells, and late apoptotic/necrotic cells, respectively. The average % population in each quadrant is indicated by the numbers at the corner of the panels.

reconfirms the observation by CLSM that both HHG2C_{18}-L and PEGHG2C_{18}-L destruct the endosomes/lysosomes successfully for cytoplasmic liberation and accomplish mitochondrial targeting. Although PEG chains relatively attenuate the strength of mitochondrial targeting of PEGHG2C_{18}-L with lower positive charge compared with HHG2C_{18}-L, PEGHG2C_{18}-L, as same as other PEGylated liposomes without PEG deshielding [40–42], have been verified for effective mitochondrial drug delivery.

3.7. Antiproliferation in vitro

The *in vitro* antiproliferation of different CCI-779-loaded liposomes against A498 cells was evaluated at pH 7.4 and pH 6.5 by MTT assay. As shown in Fig. 7, both CCI-779/HHG2C_{18}-L and CCI-779/PEGHG2C_{18}-L showed significantly enhanced antiproliferative effects at pH 6.5 relative to that at pH 7.4 ($P < 0.05$ or $P < 0.01$), and higher cytotoxicity than CCI-779/SPC-L at pH 6.5 at all the CCI-779

concentrations studied. The half maximal inhibitory concentration (IC50) of CCI-779/HHG2C18-L and CCI-779/PEGHG2C18-L were about 3 μg/mL and 5 μg/mL at pH 6.5, 1.67-fold and 1.60-fold improved relative to that at pH 7.4, respectively. However, the antiproliferation of CCI-779/SPC-L had no remarkable improvement from pH 7.4 to pH 6.5. IC50 of CCI-779/SPC-L was about 13 μg/mL at pH 7.4 and 15 μg/mL at pH 6.5. The bare $HHG2C_{18}$-L and $PEGHG2C_{18}$-L had no cytotoxicity under the same conditions up to a total lipid concentration of 5 mg/mL. It is suggested that charge conversion of $HHG2C_{18}$-L and $PEGHG2C_{18}$-L contributes to tumor cellular uptake, resulting in increased cytotoxicity at pH_e.

3.8. Cell apoptosis

Unlike antiproliferation as cell cycle arrest, apoptosis is a mechanism by which cells undergo death to control cell proliferation or in response to DNA damage [43]. The understanding of apoptosis regulated by mitochondrial pathway has provided the basis for targeted therapies of anticancer drugs that can induce death in cancer cells [44,45]. Upregulation of the PI3K/Akt/mTOR pathway is a common feature of many proliferative disorders including cancer. CCI-779, a specific inhibitor of mTOR, has been previously confirmed to have a profound effect on inducing cancer cell apoptosis [46,47]. Apart from cytosolic mTOR, a large part of mTOR associated with the regulation of cell apoptosis are situated at the mitochondrial outer membrane [48,49]. Consequently, effective transportation of CCI-779 to the mitochondria may disturb mitochondrial mTOR, thereby yielding tumor cell apoptosis.

To begin with, cell apoptosis triggered by different CCI-779-loaded liposomes was identified qualitatively by observing the morphology of the stained nuclei using fluorescence microscope. In apoptosis, condensation and fragmentation of chromatin occurs. Subsequently, nuclei lose their round or oval shape, and become crescent shape followed by fragmented-apoptotic bodies. As shown in Fig. 8, A498 cells became shrinking after incubating with different CCI-779-loaded liposomes at CCI-779 concentration of 20 μg/mL. Compared with CCI-779/SPC-L, both CCI-779/$HHG2C_{18}$-L and CCI-779/$PEGHG2C_{18}$-L presented stronger effect on promoting cell apoptosis, judged by occurrence of crescent nuclei and apoptotic bodies.

The variation of MMP, a standard for cell apoptosis, was further evaluated by JC-1 after cell incubation with different CCI-779-loaded liposomes. Based on high MMP (negative inside), JC-1 is able to specifically accumulate into the mitochondria as JC-1 aggregates exhibiting a red fluorescence, while JC-1 in the cytoplasm as a monomer shows a green fluorescence. During apoptosis of cells, MMP decreased resulting in the spillage of JC-1 from mitochondria with the increase of green fluorescence. The relative intensity between green and red fluorescence implies the decrease of MMP as the capability of breeding cell apoptosis. As shown in Fig. 9A, carbonyl cyanide m-chlorophenylhydrazone (CCCP) as a positive control led to approximately the complete loss of cellular MMP with the green fluorescence ratio of 85% after cell incubation for 0.5 h. CCCP, a mitochondrial uncoupler, can directly interfere with mitochondrial function and induce apoptosis with the deprivation of MMP. Moreover, all of various CCI-779-loaded liposomes were able to decrease MMP with increased green fluorescence ratio, compared with the blank culture media as a negative control. The rank of producing cell apoptosis effects was CCI-779/$HHG2C_{18}$-L > CCI-779/$PEGHG2C_{18}$-L > CCI-779/SPC-L (Fig. 9B), which indicates that these CCI-779 formulations are able to induce the disruption of MPP in A498 cells, thereby leading to the cell death via initiating apoptotic pathway.

Subsequently, apoptosis-inducing effect of different CCI-779-loaded liposomes was further evidenced by Annexin V-FITC/PI apoptosis detection kit. Annexin V (AV) conjugated with fluorescein isothiocyante (FITC) (AV-FITC) labels phosphatidylserine sites translocating to the extracellular membrane upon initiation of apoptosis, while PI labels the cellular DNA in the late apoptotic and necrotic cells where the cell membrane has been compromised. This combination allows the differentiation among the early apoptotic cells (AV-FITC positive, PI negative), the late apoptotic and necrotic cells (AV-FITC positive, PI positive), and the viable cells (AV-FITC negative, PI negative), and quantitative determination by flow cytometry. As shown in Fig. 10, the total apoptotic ratio of CCI-779/$HHG2C_{18}$-L increased from 9.90% at pH 7.4 to 19.53% at pH 6.5 after cell incubation for 12 h. Similarly, CCI-779/$PEGHG2C_{18}$-L showed stronger apoptosis-inducing effect at pH 6.5 (7.78%) relative to pH 7.4 (12.10%). On the contrary, there was no change in the apoptosis inducing effect of CCI-779/SPC-L at both pH values. It is demonstrated that pH-responsive $PEGHG2C_{18}$-L have pH-induced enhanced effect on promoting cell apoptosis in conformity to $HHG2C_{18}$-L.

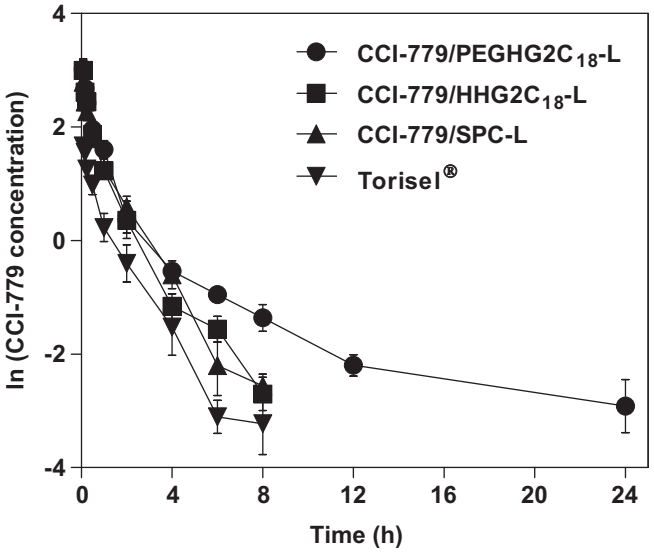

Fig. 11. Plasma concentration–time natural logarithm curves of CCI-779 after intravenous injection of various CCI-779 formulations at a dose of 10 mg/kg in rats.

According to these findings above, $HHG2C_{18}$-L and $PEGHG2C_{18}$-L can reverse their surface charge from negative to positive at pH_e for improved endocytosis, and therefore enhanced antiproliferation and cell apoptosis as well. Besides, pH_i-triggered efficient intracellular delivery, including endosomal/lysosomal escape and mitochondrial targeting, provides the interaction between CCI-779 and mitochondria, activates mitochondrial apoptotic pathway, and promotes tumor cell apoptosis.

3.9. Pharmacokinetics

Several NPs have an inconsistency between cytotoxicity *in vitro* and antitumor activity *in vivo*, in which they have superior

Table 2
Pharmacokinetic parameters of CCI-779 after intravenous injection of different CCI-779 formulations at a dose of 10 mg/kg in rats.

Parameter	CCI-779/ $PEGHG2C_{18}$-L	CCI-779/ $HHG2C_{18}$-L	CCI-779/ SPC-L	Torisel®
C_{max} (μg/mL)	20.71 ± 3.92**	20.28 ± 3.52**	16.33 ± 1.97**	5.33 ± 0.67
$AUC_{0-\infty}$ (μg h/mL)	18.06 ± 1.98**#	13.52 ± 1.71**	13.44 ± 1.57**	5.04 ± 1.10
$t_{1/2}$ (h)	5.74 ± 0.44**##	1.40 ± 0.39	1.20 ± 0.13	1.03 ± 0.12
MRT (h)	3.41 ± 0.33**##	1.20 ± 0.08	1.35 ± 0.11	1.28 ± 0.13

**$P < 0.01$ *vs* Torisel®; #$P < 0.05$, ##$P < 0.01$ *vs* CCI-779/$HHG2C_{18}$-L.

antiproliferation toward tumor cells *in vitro* but inferior inhibition of tumor *in vivo*. In addition, all investigated nanocarriers have to finally be utilized *in vivo* for cancer therapy, and their antitumor efficacies *in vivo* largely depend on their stability, bioavailability, residence time and tumor targeting in the blood circulation. Based on our previous study, compared with CCI-779/SPC-L, CCI-779/HHG2C_{18}-L had a similar pharmacokinetic profile, whereas an extremely predominant tumor inhibitive effect, verifying that multistage pH-response of HHG2C_{18}-L to pH_e and pH_i plays an evident role in delivering CCI-779 to its target for improved cancer treatment. It is noteworthy that PEGHG2C_{18}-L also exhibits the multistage pH-responsive effect on increasing tumor cellular uptake, providing effective intracellular transport, and enhancing antiproliferation and apoptosis. Accordingly, we highly focus on whether PEGHG2C_{18}-L, as PEGylated HHG2C_{18}-L, changes the pharmacokinetic profile, and reinforces the bioavailability and circulation time in blood to potentially produce much higher effect on the inhibition of tumor growth *in vivo*.

As shown in Fig. 11, CCI-779/PEGHG2C_{18}-L presented slower downtrend and gentler slope of the pharmacokinetic curves than the other three formulations including Torisel®, CCI-779/SPC-L and CCI-779/HHG2C_{18}-L, suggesting that PEGHG2C_{18}-L reduces the blood clearance and prolongs the circulating time. As shown in Table 2, both C_{max} and $AUC_{0-\infty}$ of Torisel® after intravenous administration were conspicuously lower ($P < 0.01$) than that of CCI-779-loaded liposomes, which manifests that the liposomal as encapsulating matrix of anticancer drugs package plays a remarkable role in protecting drugs away from degradation and improving the stability of the drugs. As mentioned before, there was no noticeable difference in pharmacokinetic parameters between CCI-779/HHG2C_{18}-L and CCI-779/SPC-L. In comparison with HHG2C_{18}-L, PEGHG2C_{18}-L with PEGHG2C_{18} highly increased $AUC_{0-\infty}$ to 1.34-fold, elimination half-life ($t_{1/2}$) to 4.1-fold and mean residence time (MRT) to 2.84-fold, demonstrating that it highly enhances the bioavailability and blood persistence of CCI-779, and potentially improves the therapeutic index *in vivo*.

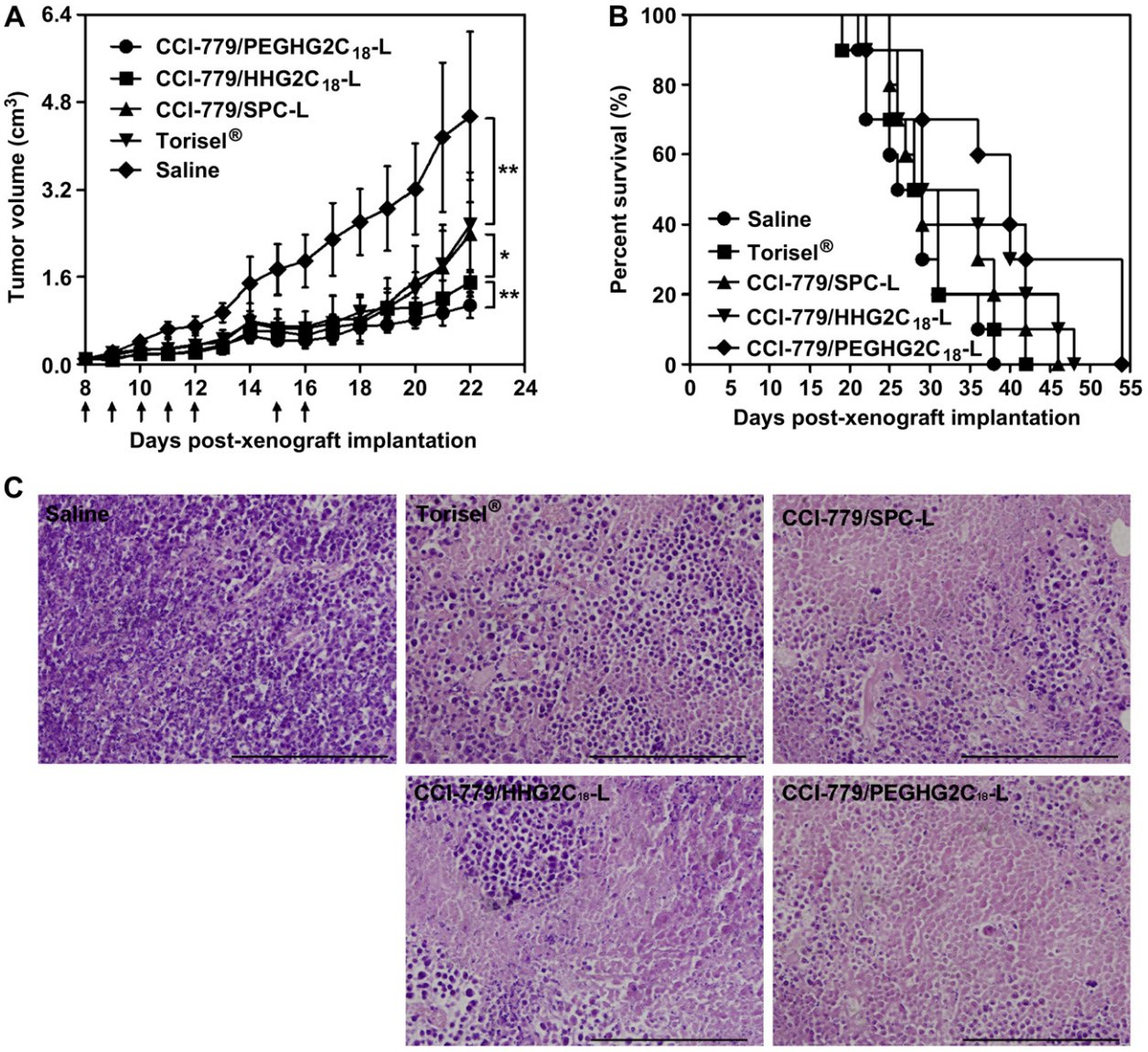

Fig. 12. *In vivo* therapeutic efficacy of various CCI-779 formulations in Renca tumor-bearing mice. (A, B) Changes of tumor volumes (A) and survival rates (B) of tumor-bearing mice after intravenous injection of different CCI-779 formulations at a dose of 10 mg/kg and saline as a negative control. The arrows signify the time of intravenous administration. $^{*}P < 0.05$, $^{**}P < 0.01$. (C) Representative images of tumor sections separated from mice stained by HE at 22 days post-implantation. Scale bars are 200 μm.

3.10. Antitumor efficacy in vivo

In order to confirm the feasibility of PEGHG2C$_{18}$-L for cancer therapy *in vivo*, Renca tumor xenograft models were used to evaluate the *in vivo* antitumor efficacy of CCI-779/PEGHG2C$_{18}$-L. As shown in Fig. 12A, all of the CCI-779 formulations significantly reduced the tumor volumes compared with saline as a negative control. However, no evident difference was found in the tumor volumes of tumor-bearing mice after successive intravenous administration of Torisel® and CCI-779/SPC-L. However, CCI-779/HHG2C$_{18}$-L, with the similar pharmacokinetic profile of CCI-779/SPC-L, displayed a prominent effect on tumor-size inhibition compared with Torisel® ($P < 0.01$) and CCI-779/SPC-L ($P < 0.05$). The results demonstrate that preferable interactions with tumor cells, such as electrostatic binding by charge conversion and effective intracellular delivery are crucial prerequisites for the liposomes to have a superior antitumor efficacy *in vivo*, although the liposomes have the EPR effect for passive tumor targeting compared with the drug solution. More importantly, CCI-779/PEGHG2C$_{18}$-L behaved much higher tumor inhibitive effect ($P < 0.01$) than CCI-779/HHG2C$_{18}$-L. Furthermore, CCI-779/PEGHG2C$_{18}$-L possessed the most distinguished effect on extending the survival period of the tumor-bearing mice (Fig. 12B), and no evident reduction of the body weight of the tumor-bearing mice has been found during the study (Fig. S4). The images of the stained tumor tissue section by hematoxylin and eosin (HE) also showed the greatest massive cancer cell remission after applying CCI-779/PEGHG2C$_{18}$-L (Fig. 12C), which presents a substantial evidence of the highest antitumor activity of CCI-779/PEGHG2C$_{18}$-L *in vivo*. Overall, PEGHG2C$_{18}$-L, dually decorated with HHG2C$_{18}$ and PEGHG2C$_{18}$, can improve the stability, bioavailability and persistence in the blood circulation, increase the accumulation at the tumor site by the EPR effect and charge conversion, enhance the tumor cellular uptake, realize the effective intracellular delivery, and thereby achieve the optimal antitumor efficacy *in vivo*.

4. Conclusion

In summary, we developed pH-sensitive liposomes (HHG2C$_{18}$-L and PEGHG2C$_{18}$-L) based on zwitterionic oligopeptide lipids for tumor-targeted anticancer drug delivery. Both of them have the capability of charge conversion to the surrounding pH for increased tumor cellular uptake at pH$_e$, and the effect on endosomal/lysosomal escape and mitochondrial targeting for enhanced antiproliferation and apoptosis. Indeed, PEGHG2C$_{18}$-L displayed higher blood persistence and antitumor efficacy in comparison with HHG2C$_{18}$-L. Our findings indicate that HHG2C$_{18}$-L and PEGHG2C$_{18}$-L as pH-sensitive liposomes are highly effective drug carriers for providing both efficient intracellular drug delivery and blood circulation. Additionally, more work is being performed in our group on further incorporation of PEGylated zwitterionic oligopeptide lipids with pH$_e$-induced PEG deshielding function into these nanoplatforms to achieve more advanced development for cancer therapy.

Acknowledgement

This work is financially supported by the National Natural Science Foundation of China (81072589) and 111 Project from the Ministry of Education of China and the State Administration of Foreign Expert Affairs of China (No. 111-2-07).

Appendix A. Supplementary data

Supplementary data related to this article can be found at http://dx.doi.org/10.1016/j.biomaterials.2013.01.030.

References

[1] Torchilin VP. Recent advances with liposomes as pharmaceutical carriers. Nat Rev Drug Discov 2005;4:145–60.
[2] Wang H, Zhao P, Liang X, Gong X, Song T, Niu R, et al. Folate-PEG coated cationic modified chitosan–cholesterol liposomes for tumor-targeted drug delivery. Biomaterials 2010;31:4129–38.
[3] Jiang T, Zhang Z, Zhang Y, Lv H, Zhou J, Li C, et al. Dual-functional liposomes based on pH-responsive cell-penetrating peptide and hyaluronic acid for tumor-targeted anticancer drug delivery. Biomaterials 2012;33:9246–58.
[4] Barenholz Y. Doxil®-the first FDA-approved nano-drug: lessons learned. J Control Release 2012;160:117–34.
[5] Fassas A, Anagnostopoulos A. The use of liposomal daunorubicin (DaunoXome) in acute myeloid leukemia. Leuk Lymphoma 2005;46:795–802.
[6] Narang AS, Varia S. Role of tumor vascular architecture in drug delivery. Adv Drug Deliv Rev 2011;63:640–58.
[7] Un K, Sakai-Kato K, Oshima Y, Kawanishi T, Okuda H. Intracellular trafficking mechanism, from intracellular uptake to extracellular efflux, for phospholipid/cholesterol liposomes. Biomaterials 2012;33:8131–41.
[8] Bareford LM, Swaan PW. Endocytic mechanisms for targeted drug delivery. Adv Drug Deliv Rev 2007;59:748–58.
[9] Zohra FT, Chowdhury EH, Akaike T. High performance mRNA transfection through carbonate apatite–cationic liposome conjugates. Biomaterials 2009;30:4006–13.
[10] Koynova R, Wang L, MacDonald RC. An intracellular lamellar–nonlamellar phase transition rationalizes the superior performance of some cationic lipid transfection agents. Proc Natl Acad Sci U S A 2006;103:14373–8.
[11] Yamada Y, Harashima H. Delivery of bioactive molecules to the mitochondrial genome using a membrane-fusing, liposome-based carrier, DF-MITO-Porter. Biomaterials 2012;33:1589–95.
[12] Chan CL, Majzoub RN, Shirazi RS, Ewert KK, Chen YJ, Liang KS, et al. Endosomal escape and transfection efficiency of PEGylated cationic liposome–DNA complexes prepared with an acid-labile PEG-lipid. Biomaterials 2012;33:4928–35.
[13] Shigeta K, Kawakami S, Higuchi Y, Okuda T, Yagi H, Yamashita F, et al. Novel histidine-conjugated galactosylated cationic liposomes for efficient hepatocyte-selective gene transfer in human hepatoma HepG2 cells. J Control Release 2007;118:262–70.
[14] Dehshahri A, Oskuee RK, Shier WT, Hatefi A, Ramezani M. Gene transfer efficiency of high primary amine content, hydrophobic, alkyl-oligoamine derivatives of polyethylenimine. Biomaterials 2009;30:4187–94.
[15] Soenen SJ, Brisson AR, De Cuyper M. Addressing the problem of cationic lipid-mediated toxicity: the magnetoliposome model. Biomaterials 2009;30:3691–701.
[16] Moore NM, Barbour TR, Sakiyama-Elbert SE. Synthesis and characterization of four-arm poly(ethylene glycol)-based gene delivery vehicles coupled to integrin and DNA-binding peptides. Mol Pharm 2008;5:140–50.
[17] Rodrigues PC, Beyer U, Schumacher P, Roth T, Fiebig HH, Unger C, et al. Acid-sensitive polyethylene glycol conjugates of doxorubicin: preparation, in vitro efficacy and intracellular distribution. Bioorg Med Chem 1999;7:2517–24.
[18] Sawant RM, Hurley JP, Salmaso S, Kale A, Tolcheva E, Levchenko TS, et al. "SMART" drug delivery systems: double-targeted pH-responsive pharmaceutical nanocarriers. Bioconjug Chem 2006;17:943–9.
[19] Prabaharan M, Grailer JJ, Pilla S, Steeber DA, Gong S. Amphiphilic multi-arm-block copolymer conjugated with doxorubicin via pH-sensitive hydrazone bond for tumor-targeted drug delivery. Biomaterials 2009;30:5757–66.
[20] Obata Y, Tajima S, Takeoka S. Evaluation of pH-responsive liposomes containing amino acid-based zwitterionic lipids for improving intracellular drug delivery in vitro and in vivo. J Control Release 2010;142:267–76.
[21] Mo R, Sun Q, Xue J, Li N, Li W, Zhang C, et al. Multistage pH-responsive liposomes for mitochondrial-targeted anticancer drug delivery. Adv Mater 2012;24:3659–65.
[22] Perry JW, Wobus CE. Endocytosis of murine norovirus 1 into murine macrophages is dependent on dynamin II and cholesterol. J Virol 2010;84:6163–76.
[23] Durymanov MO, Beletkaia EA, Ulasov AV, Khramtsov YV, Trusov GA, Rodichenko NS, et al. Subcellular trafficking and transfection efficacy of polyethylenimine-polyethylene glycol polyplex nanoparticles with a ligand to melanocortin receptor-1. J Control Release 2012;163:211–9.
[24] Koivusalo M, Welch C, Hayashi H, Scott CC, Kim M, Alexander T, et al. Amiloride inhibits macropinocytosis by lowering submembranous pH and preventing Rac1 and Cdc42 signaling. J Cell Biol 2010;188:547–63.
[25] Kommareddy S, Amiji M. Poly(ethylene glycol)-modified thiolated gelatin nanoparticles for glutathione-responsive intracellular DNA delivery. Nanomedicine 2007;3:32–42.
[26] Choi KY, Min KH, Yoon HY, Kim K, Park JH, Kwon IC, et al. PEGylation of hyaluronic acid nanoparticles improves tumor targetability in vivo. Biomaterials 2011;32:1880–9.
[27] Kohli E, Han HY, Zeman AD, Vinogradov SV. Formulations of biodegradable nanogel carriers with 5′-triphosphates of nucleoside analogs that display a reduced cytotoxicity and enhanced drug activity. J Control Release 2007;121:19–27.
[28] Oumzil K, Khiati S, Grinstaff MW, Barthélémy P. Reduction-triggered delivery using nucleoside-lipid based carriers possessing a cleavable PEG coating. J Control Release 2011;151:123–30.

[29] Li SD, Huang L. Stealth nanoparticles: high density but sheddable PEG is a key for tumor targeting. J Control Release 2010;145:178–81.
[30] Xu P, Van Kirk EA, Zhan Y, Murdoch WJ, Radosz M, Shen Y. Targeted charge-reversal nanoparticles for nuclear drug delivery. Angew Chem Int Ed Engl 2007;46:4999–5002.
[31] Lee Y, Ishii T, Cabral H, Kim HJ, Seo JH, Nishiyama N, et al. Charge-conversional polyionic complex micelles-efficient nanocarriers for protein delivery into cytoplasm. Angew Chem Int Ed Engl 2009;48:5309–12.
[32] Yue ZG, Wei W, Lv PP, Yue H, Wang LY, Su ZG, et al. Surface charge affects cellular uptake and intracellular trafficking of chitosan-based nanoparticles. Biomacromolecules 2011;12:2440–6.
[33] Koren E, Apte A, Jani A, Torchilin VP. Multifunctional PEGylated 2C5-immunoliposomes containing pH-sensitive bonds and TAT peptide for enhanced tumor cell internalization and cytotoxicity. J Control Release 2012; 160:264–73.
[34] Nie Y, Günther M, Gu Z, Wagner E. Pyridylhydrazone-based PEGylation for pH-reversible lipopolyplex shielding. Biomaterials 2011;32:858–69.
[35] Khalil IA, Kogure K, Futaki S, Harashima H. High density of octaarginine stimulates macropinocytosis leading to efficient intracellular trafficking for gene expression. J Biol Chem 2006;281:3544–51.
[36] Yamada Y, Furukawa R, Yasuzaki Y, Harashima H. Dual function MITO-Porter, a nano carrier integrating both efficient cytoplasmic delivery and mitochondrial macromolecule delivery. Mol Ther 2011;19:1449–56.
[37] Midoux P, Pichon C, Yaouanc JJ, Jaffrès PA. Chemical vectors for gene delivery: a current review on polymers, peptides and lipids containing histidine or imidazole as nucleic acids carriers. Br J Pharmacol 2009;157:166–78.
[38] Lee ES, Na K, Bae YH. Super pH-sensitive multifunctional polymeric micelle. Nano Lett 2005;5:325–9.
[39] Wen Y, Guo Z, Du Z, Fang R, Wu H, Zeng X, et al. Serum tolerance and endosomal escape capacity of histidine-modified pDNA-loaded complexes based on polyamidoamine dendrimer derivatives. Biomaterials 2012;33:8111–21.
[40] Wang XX, Li YB, Yao HJ, Ju RJ, Zhang Y, Li RJ, et al. The use of mitochondrial targeting resveratrol liposomes modified with a dequalinium polyethylene glycol–distearoylphosphatidyl ethanolamine conjugate to induce apoptosis in resistant lung cancer cells. Biomaterials 2011;32:5673–87.
[41] Zhang L, Yao HJ, Yu Y, Zhang Y, Li RJ, Ju RJ, et al. Mitochondrial targeting liposomes incorporating daunorubicin and quinacrine for treatment of relapsed breast cancer arising from cancer stem cells. Biomaterials 2012;33:565–82.
[42] Biswas S, Dodwadkar NS, Deshpande PP, Torchilin VP. Liposomes loaded with paclitaxel and modified with novel triphenylphosphonium-PEG-PE conjugate possess low toxicity, target mitochondria and demonstrate enhanced antitumor effects in vitro and in vivo. J Control Release 2012;159:393–402.
[43] Lowe SW, Lin AW. Apoptosis in cancer. Carcinogenesis 2000;21:485–95.
[44] Biasutto L, Dong LF, Zoratti M, Neuzil J. Mitochondrially targeted anti-cancer agents. Mitochondrion 2010;10:670–81.
[45] Wenner CE. Targeting mitochondria as a therapeutic target in cancer. J Cell Physiol 2012;227:450–6.
[46] Ghobrial IM, Witzig TE, Adjei AA. Targeting apoptosis pathways in cancer therapy. CA Cancer J Clin 2005;55:178–94.
[47] Vignot S, Faivre S, Aguirre D, Raymond E. mTOR-targeted therapy of cancer with rapamycin derivatives. Ann Oncol 2005;16:525–37.
[48] Desai BN, Myers BR, Schreiber SL. FKBP12-rapamycin-associated protein associates with mitochondria and senses osmotic stress via mitochondrial dysfunction. Proc Natl Acad Sci U S A 2002;99:4319–24.
[49] Ramanathan A, Schreiber SL. Direct control of mitochondrial function by mTOR. Proc Natl Acad Sci U S A 2009;106:22229–32.